INFRARED INDICES OF REFRACTION AND REFLECTIVITIES OF Mg_2Si, Mg_2Ge AND Mg_2Sn

by

Donald Arthur McWilliams

A Dissertation Submitted to the
Graduate Faculty in Partial Fulfillment of
The Requirements for the Degree of
DOCTOR OF PHILOSOPHY

Major Subject: Physics

Approved:

Signature was redacted for privacy.

In Charge of Major Work

Signature was redacted for privacy.

Head of Major Department

Signature was redacted for privacy.

Dean of Graduate College

Iowa State University
Of Science and Technology
Ames, Iowa

1962

TABLE OF CONTENTS

		Page
I.	INTRODUCTION	1
II.	DETERMINATION OF THE INDEX OF REFRACTION IN THE INFRARED	8
III.	MEASUREMENT OF REFLECTIVITY	23
IV.	REFLECTIVITY RESULTS	30
V.	DISCUSSION	34
VI.	BIBLIOGRAPHY	47
VII.	ACKNOWLEDGMENTS	50
VIII.	APPENDIX A: LIST OF SYMBOLS	51
IX.	APPENDIX B: CLASSICAL OSCILLATOR EQUATIONS WITH FIGURES AND PRINTED COMPUTER SOLUTIONS	53
X.	APPENDIX C: INDEX OF REFRACTION DETERMINATION DATA	60
XI.	APPENDIX D: REFLECTIVITY DETERMINATION DATA	63

LIST OF FIGURES

		Page
Figure 1.	Apparatus for determining the index of refraction by minimum deviation	9
Figure 2.	Index of refraction versus wavelength for NaCl III prism	12
Figure 3.	Index of refraction versus wavelength for Si III prism	13
Figure 4.	Index of refraction versus wavelength for a Ge prism	14
Figure 5.	Index of refraction versus wavelength for Mg_2Si III prism	15
Figure 6.	Index of refraction versus wavelength for Mg_2Si III prism	16
Figure 7.	Index of refraction versus wavelength for Mg_2Ge I prism	18
Figure 8.	Index of refraction versus wavelength for Mg_2Sn I prism	20
Figure 9.	Summary of index of refraction measurements	21
Figure 10.	Apparatus for the reflectivity determination	24
Figure 11.	Reflectivity of NaCl	28
Figure 12.	Reflectivity of Mg_2Si	31
Figure 13.	Reflectivity of Mg_2Ge	32
Figure 14.	Reflectivity of Mg_2Sn with different carrier concentrations	33
Figure 15.	Reflectivity of a classical oscillator compared to the reflectivity of Mg_2Si II	35
Figure 16.	Reflectivity of a classical oscillator compared with the reflectivity of Mg_2Si II	36

Page

Figure 17. Reflectivity of a classical oscillator compared with the reflectivity of Mg_2Ge I 37

Figure 18. Reflectivity versus wavelength for p-doped Mg_2Ge and a classical oscillator with free carrier modifications 41

Figure 19. Reflectivity of the Mg compounds versus energy 44

Figure 20. Extinction coefficient versus wavelength for a classical oscillator 55

Figure 21. Susceptibility versus wavelength for a classical oscillator 56

Figure 22. Conductivity/frequency versus wavelength for a classical oscillator 57

Figure 23. Index of refraction versus wavelength for a classical oscillator 58

Figure 24. Approximate wavelength calibration for a 12° CsI prism in the Perkin-Elmer Model 160 monochromator 68

LIST OF TABLES

		Page
Table 1.	Refractive index of Mg_2Si III	17
Table 2.	Refractive index of Mg_2Ge I	19
Table 3.	Refractive index of Mg_2Sn I	22
Table 4.	Wavelength ranges, prisms and filtering techniques	26
Table 5.	Computer solution for a classical oscillator	59
Table 6.	Sextant calibration	60
Table 7.	Minimum deviation data for Mg_2Sn I	60
Table 8.	Minimum deviation data for Mg_2Si III	61
Table 9.	Minimum deviation data for Mg_2Ge I	62
Table 10.	Reflectivity data - CsI prism	64

I. INTRODUCTION

A. Purpose of This Experiment

This work was undertaken with the hope that some new light could be cast on the properties of Mg_2Si, Mg_2Ge and Mg_2Sn. The optical properties of many semiconducting materials have been summarized by Moss (1). In semiconductors the optical properties have been very useful in determining, typically, the mechanisms of electrical conduction, the structure of the energy gap, the interatomic forces in the crystals, the surface properties of the materials, the effective masses of the carriers and the mechanisms of light absorption and photoconductivity.

The primary purpose of this experiment was to add to current knowledge of these Mg compounds. In particular, the effective mass of the carriers might be determined from the index of refraction or the reflectivity. Simultaneously, one might obtain the optical dielectric constant and the static dielectric constant, with the difference of these giving the ionicity. The optical data for the Mg compounds could be compared with other materials for similarities or differences. An indication of the effect of the atomic lattice on the reflectivity would give useful information to people studying the interatomic forces in the Mg compounds and other materials.

B. Previous Work

The preparation and electrical properties of Mg_2Si have been discussed by Morris (2) and Whitsett (3); of Mg_2Ge by Redin (4); of Mg_2Sn by Blunt et al. (5). The optical transmission of Mg_2Ge and Mg_2Si was discussed by Koenig et al. (6); of Mg_2Sn by Blunt et al. (5).

Several people have made Hall effect measurements on the Mg compounds and have obtained estimates for the effective masses of the carriers. Morris (2) reported the effective mass of electrons, m_e^*, in Mg_2Si as 0.46 m, where m is the mass of the electron. He also reported $m_h^* = 0.87$ m where m_h^* is the effective mass of the hole. His work differs from Winkler's (7) results, which were $m_e^* = 0.36$ m and $m_h^* = 0.72$ m. Redin (4) studied Mg_2Ge and gave $m_e^* = 0.18$ m and $m_h^* = 0.31$ m. All of these people report a lack of confidence in the values reported due to the number of assumptions made. Blunt et al. (5) reported $m_e^* = 1.17$ m and $m_h^* = 1.28$ m for Mg_2Sn.

Heller (8) studied the Seebeck effect in Mg_2Si and obtained $m_e^* \approx 0.5$ m and $m_h^* \approx 2$ m. There is also reason for uncertainty in these values.

There seems to be no previous reported work on the determination of the indices of refraction or the reflection spectra of these compounds in the infrared region. It is

possible, using an approximation given by Moss (9, p. 61), to arrive at an approximate value for the optical dielectric constant based on observations of the energy gap in different semiconducting materials. Moss notes that for many semiconducting materials the product of the dielectric constant squared and the energy gap is equal to a constant value. Madelung (10) obtained a value of 155 on an average of 8 values for different materials. Using Madelung's average, with an energy gap of 0.78 ev obtained by Morris (2) for Mg_2Si, one obtains $\epsilon = 14$ for Mg_2Si. Morris (2), using this value of ϵ in his analysis of the mobility of Mg_2Si, obtained reasonable agreement between theory and experiment.

C. Remarks on the Theory of Optical Measurements

A general discussion of the optical properties of semiconductors is given by Moss (1); the notation in this paper agrees with his and is given in Appendix A. All expressions and data are in MKS units.

In vacuum the electric field of a light wave can be written in the form

$$E = E_o \exp i\omega\left(\frac{x}{c} - t\right)$$

where E_o is a constant called the amplitude, $\frac{\omega}{2\pi}$ is the frequency, x is the displacement of the wave parallel to the

motion of the light wave, t is the time and c is the speed of light. Inside isotropic matter the light wave can be expressed as

$$E = E_o \exp i\, \omega(\frac{\underline{N}x}{c} - t) .$$

Allowing for the possibility that $\underline{N}$ is complex, one usually writes

$$\underline{N} = n - ik$$

where n is the index of refraction and k is the extinction coefficient. $\underline{N}^2$, of course, is complex and

$$\underline{N}^2 = n^2 - k^2 - 2\, i\, n\, k .$$

Maxwell's equations for a conducting medium can be solved to show that the dielectric constant is $n^2 - k^2$ and $2nk = \frac{\sigma}{\omega \epsilon_o}$, where σ is the conductivity [Moss (1, p. 1)].

The measurement of the index of refraction, n, of a material can yield the optical dielectric constant, ϵ, since, when the extinction coefficient, k, is small compared with n, as it must be in any transparent crystal,

$$\epsilon = n^2 - k^2 \approx n^2 .$$

In the transparent region k is quite small, as can be seen from the relationship between K, the absorption coefficient, and k.

$$K = \frac{4\pi k}{\lambda} .$$

λ is the wavelength of the incident light. A crystal 1 millimeter thick transmitting 0.01 of the incident light would have a value of K = 4600 per meter. With $\lambda = 5$ microns, $k = 1.83 \times 10^{-3}$, which is quite small compared with typical values of n which are greater than 1.0.

Similarly, when $k \ll n$, n and ϵ can be determined from the normal reflectivity, R, which is given by the expression [Moss (1, p. 6)]

$$R = \frac{(n - 1)^2 + k^2}{(n + 1)^2 + k^2} .$$

In the region where changes in n and R are due only to free carriers, one can determine the effective mass, m^*, of the carriers by using the classical equations of motion of a particle under the influence of an oscillating field. The appropriate equation [Moss (1, p. 236)] is

$$n^2 - k^2 = \epsilon - \frac{Ne^2}{m^* \mathcal{E}_o \omega^2} .$$

Here ϵ is the near infrared dielectric constant and $\mathcal{E}_o$ is the dielectric constant of free space. A determination of the effective mass could not be made for the studied Mg compounds because the influence of the atomic lattice on the reflectivity was pronounced and the free carrier contribution could not be evaluated.

In addition to the free carrier contribution to the optical properties of solids, one finds that electromagnetic radiation interacts with bound charges in the atomic lattice. In a classical sense the electric field of the light induces motion of the ions in the lattice. Kittel (11, p. 103) discusses the elementary arguments which lead to the possible ways (modes) in which these atoms may move with respect to one another. He shows how a local charge separation (electric dipole moment) can occur with which an incident electromagnetic wave can interact. Whitten (12) has studied Mg_2Si and gives for the modes with a dipole moment (optical mode) in the limit of long phonon wavelengths

$$\mu\omega^2 = f .$$

μ is the reduced mass of the unit cell, $\frac{\omega}{2\pi}$ is the frequency of the mode and f is a function of the restoring forces in the crystal. f can have two values. One of these values corresponds to a transverse mode of vibration and the other to a longitudinal mode. Incident light, being a transverse wave, cannot interact with the longitudinal optical mode. However, Lyddane, Sachs and Teller [Fröhlich (13)] have derived a relation between the frequencies of the two modes.

$$\omega_L = \left(\frac{\epsilon}{\epsilon_o}\right)^{1/2} \omega_r$$

where ϵ_o is the static dielectric constant, ϵ the near

infrared dielectric constant, ω_T the frequency of the transverse optical mode and ω_L the frequency of the longitudinal optical mode.

The longitudinal optical mode cannot be detected with light, but it does interact with charges inside the lattice, and contributes to the electrical resistance of a crystal by interacting with the current carriers. The frequency of the longitudinal mode enters into the calculation of the optical mode scattering by polar crystals and is discussed by Ziman (14, p. 434).

Additionally, an estimate can be made of an upper limit to ϵ_o, the static dielectric constant, by examining the reflectivity of a pure crystal on the long wavelength side of ω_T. As is shown in Appendix B, k for a classical oscillator drops to a small value at long wavelengths. If the influence of free carriers is neglected, the index of refraction, determined from the limiting value of the reflectivity, should be close to $\epsilon^{1/2}$. With semiconductors, it is not possible to ignore the contribution of free carriers to the reflectivity since k for free carriers becomes larger as the frequency of the incident light decreases and may not be negligible in the reflectivity equations. A qualitative understanding of this conclusion is indicated by the equation relating n, k and σ, the conductivity, [Moss (1, p. 2)].

$$2nk = \frac{\sigma}{\omega \epsilon_o}$$

or

$$k = \frac{\sigma}{2n\,\omega \epsilon_o} .$$

This shows that k can get quite large as ω decreases.

It is not yet possible to grow crystals of the Mg compounds pure enough to obtain even an approximation to ϵ_o. It is only possible to establish an upper limit to ϵ_o. The high conductivity also prevents the determination of ϵ_o by electrical means.

II. DETERMINATION OF THE INDEX OF REFRACTION IN THE INFRARED

A. Experimental Technique

This experiment obtained the indices of refraction of prisms of Mg_2Si, Mg_2Ge and Mg_2Sn by the minimum deviation method. A diagram of the equipment is shown in Figure 1. A standard Perkin-Elmer monochromator was modified to accommodate a collimator, sample holder and movable detector. Light from a Globar was passed through a 13 cycles-per-second chopper and reflected from a flat mirror to a source-focusing mirror focused on the entrance slit of a NaCl monochromator. Light passing from the exit slit of the monochromator was incident on a focusing mirror called a receiving mirror. This mirror, in combination with the collimating mirror, caused the light beam from the exit slit to be collimated in the horizontal plane. The beam was then reflected to the sample by the small flat extraction mirror. Although the light did diverge vertically through the prism, the precision of the Si index of refraction determination indicates the curvature of the beam was negligible. After leaving the sample prism, which could be rotated to obtain minimum deviation, the light passed through two defining slits as shown in Figure 1 before being focused on the thermocouple detector by the detector mirror. The angle at which

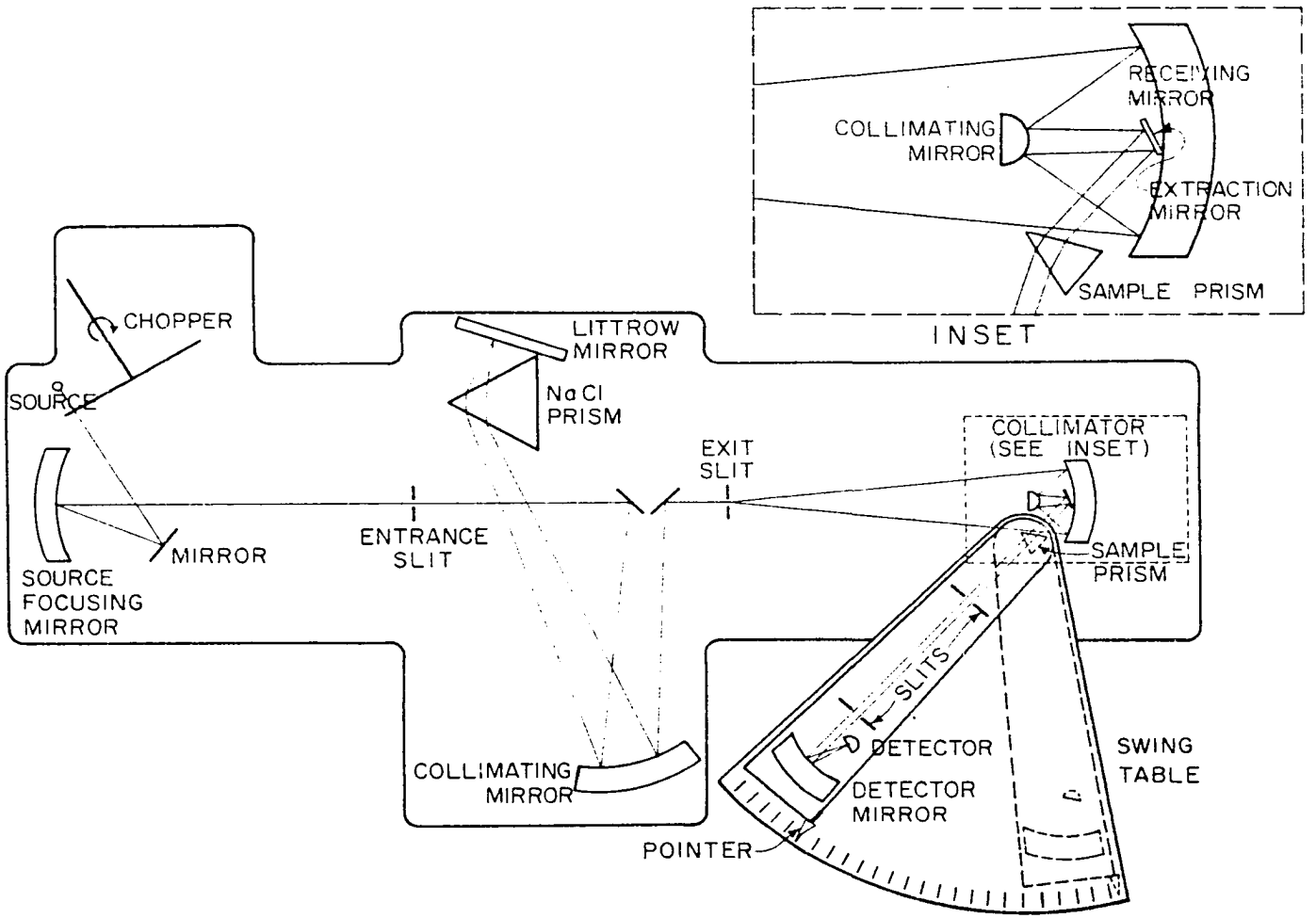

Figure 1. Apparatus for determining the index of refraction by minimum deviation

the refracted beam was detected was measured on the swing table and the point of maximum light was determined by the excursion of a Brown potentiometer driven by a Perkin-Elmer amplifier.

The sample was glued to a holder and ground with emery paper to the proper dimension (approximately 10°). The prism was then polished with Al_2O_3 on a nap cloth. The sample prism was mounted on a small brass table with clay and a standard spectrometer was used to determine the prism apex angle. A slit, illuminated with white light, was imaged in the eyepiece of the spectrometer by reflection from alternate sides of the mounted sample prism centered on the spectrometer table. The rotation angle of the spectrometer table could be read to 20 seconds of arc and the difference of the two readings obtained from opposite sides of the prism was used as the effective apex angle of the sample prism. This measurement gave the apex angle with an error of less than 1 minute. The prism and the prism table were then transferred to the monochromator swing table and a minimum deviation determination was done. The swing table arc was calibrated to $\pm$ 2 minutes of arc. The data thus obtained were substituted in the minimum deviation equation

$$n = \frac{\sin (\alpha + \delta)/2}{\sin \delta/2}$$

where δ is the apex angle and α is the angle of minimum deviation. One can see that it is important to measure the effective apex angle accurately when it is small.

The equipment was tested by running various prisms of different materials. Prisms of NaCl, Si and Ge were made and measured with the same technique used for the prisms of Mg_2Si, Mg_2Ge and Mg_2Sn.

Figure 2 shows the comparison of four datum points from NaCl prism III with the data of Coblentz (15). Several Si prisms were run. Silicon prism III is a prism made of Dow Corning hyper-pure p-type Si with 2500 Ohm-centimeters resistivity. The values for the index of refraction obtained on this equipment are compared in Figure 3 with the data of Salzberg and Villa (16). Similarly, a Ge prism of unknown purity is compared in Figure 4 with the data of Salzberg and Villa (16).

B. Experimental Results

The values obtained for the index of refraction of Mg_2Si III are given in Table 1. These values are plotted in Figure 5. The high absorption of the prism in the long wavelength region made it necessary to use wide slits. This decreased the precision of the determination because the beam was not collimated when wide slits were used. Figure 6 shows the data of Mg_2Si III in an expanded plot which gives a better

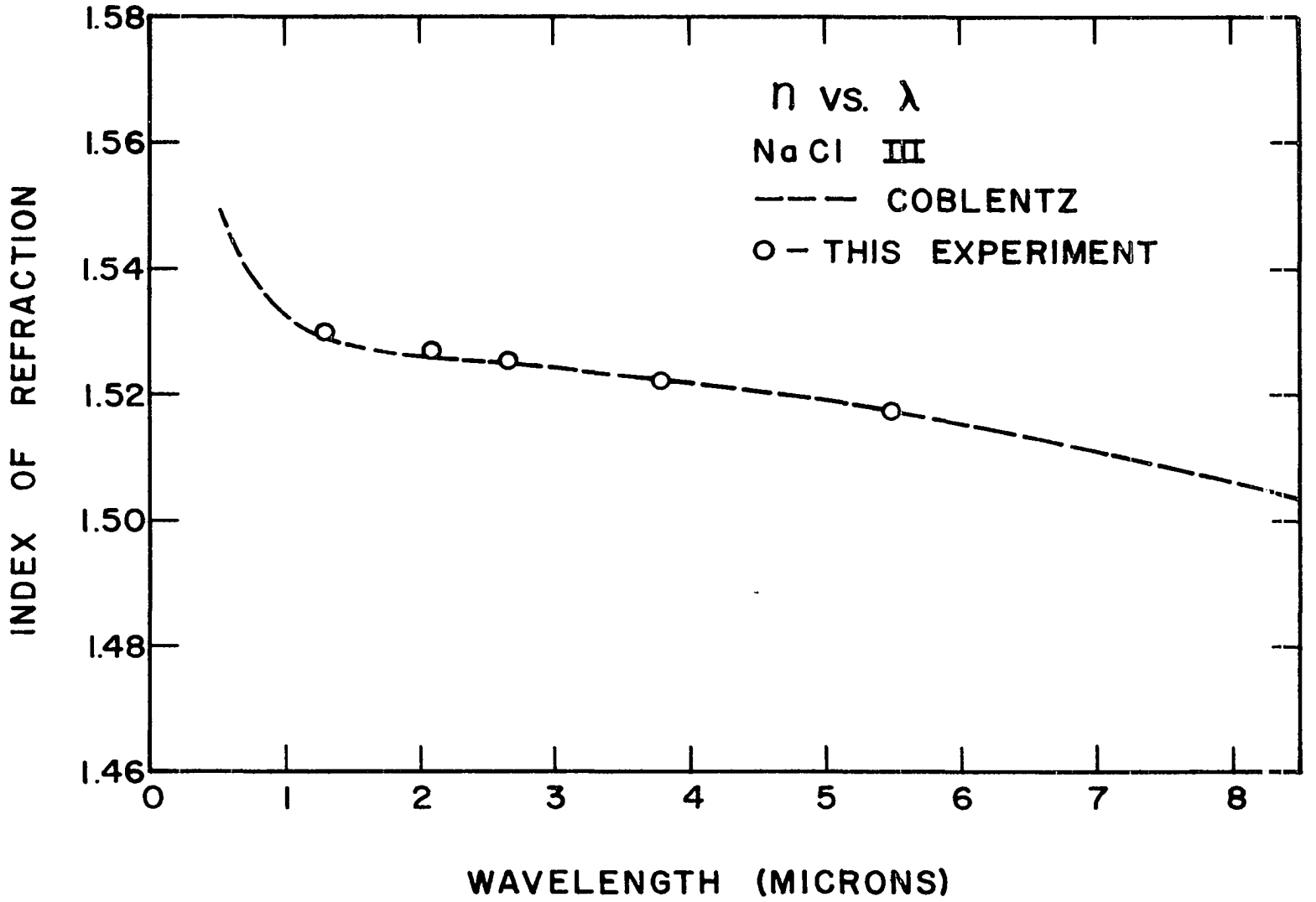

Figure 2. Index of refraction versus wavelength for NaCl III prism

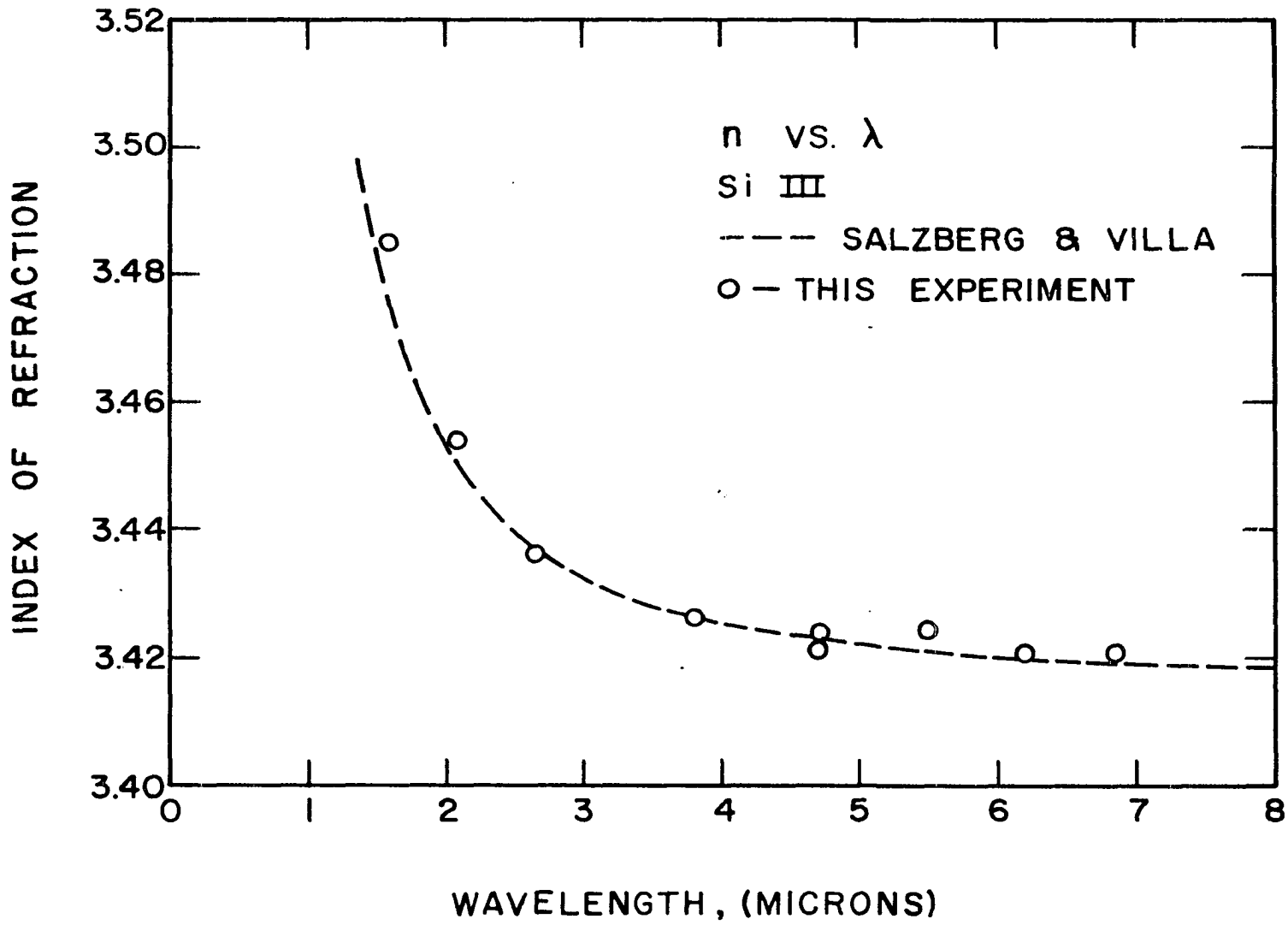

Figure 3. Index of refraction versus wavelength for Si III prism

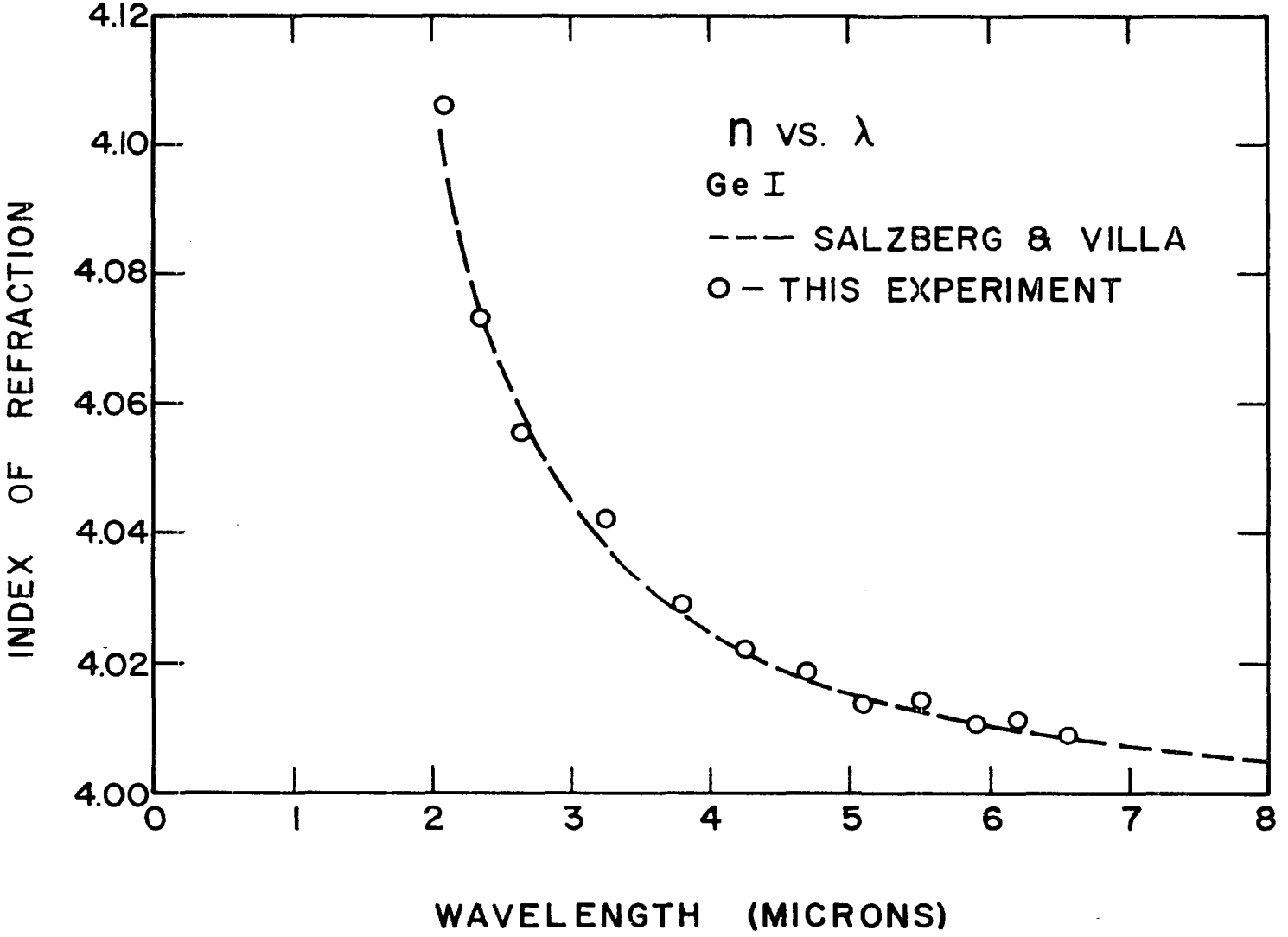

Figure 4. Index of refraction versus wavelength for a Ge prism

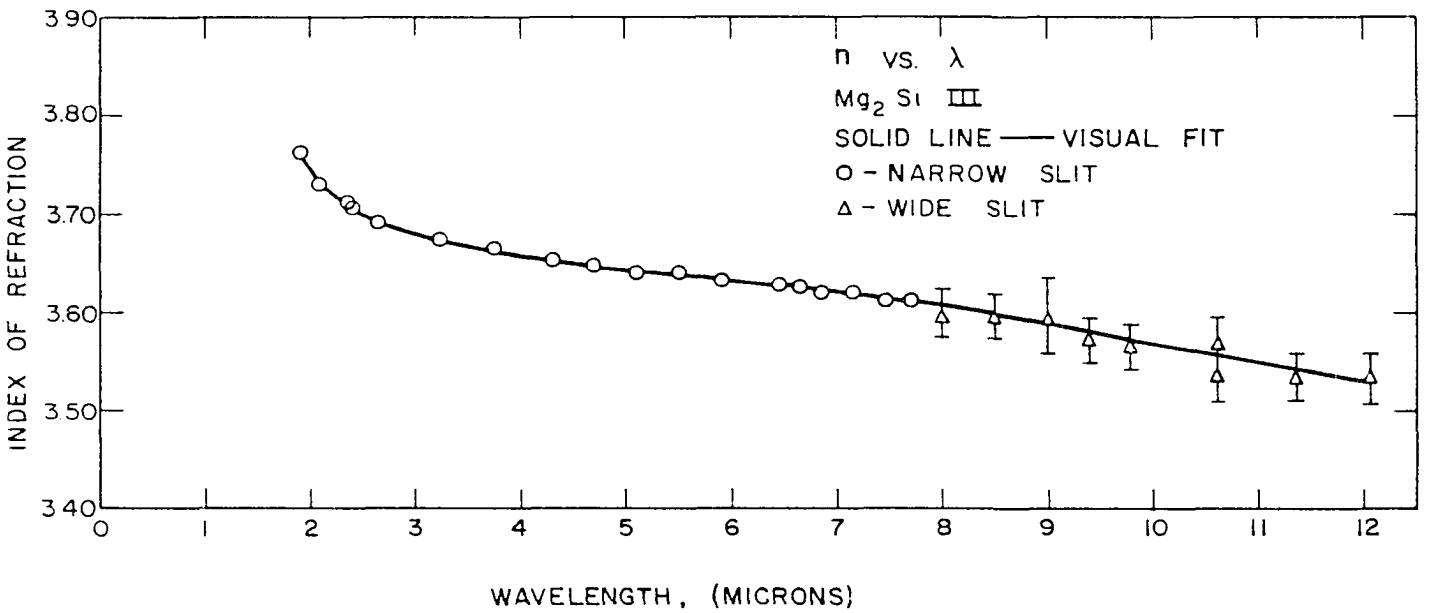

Figure 5. Index of refraction versus wavelength for Mg_2Si III prism

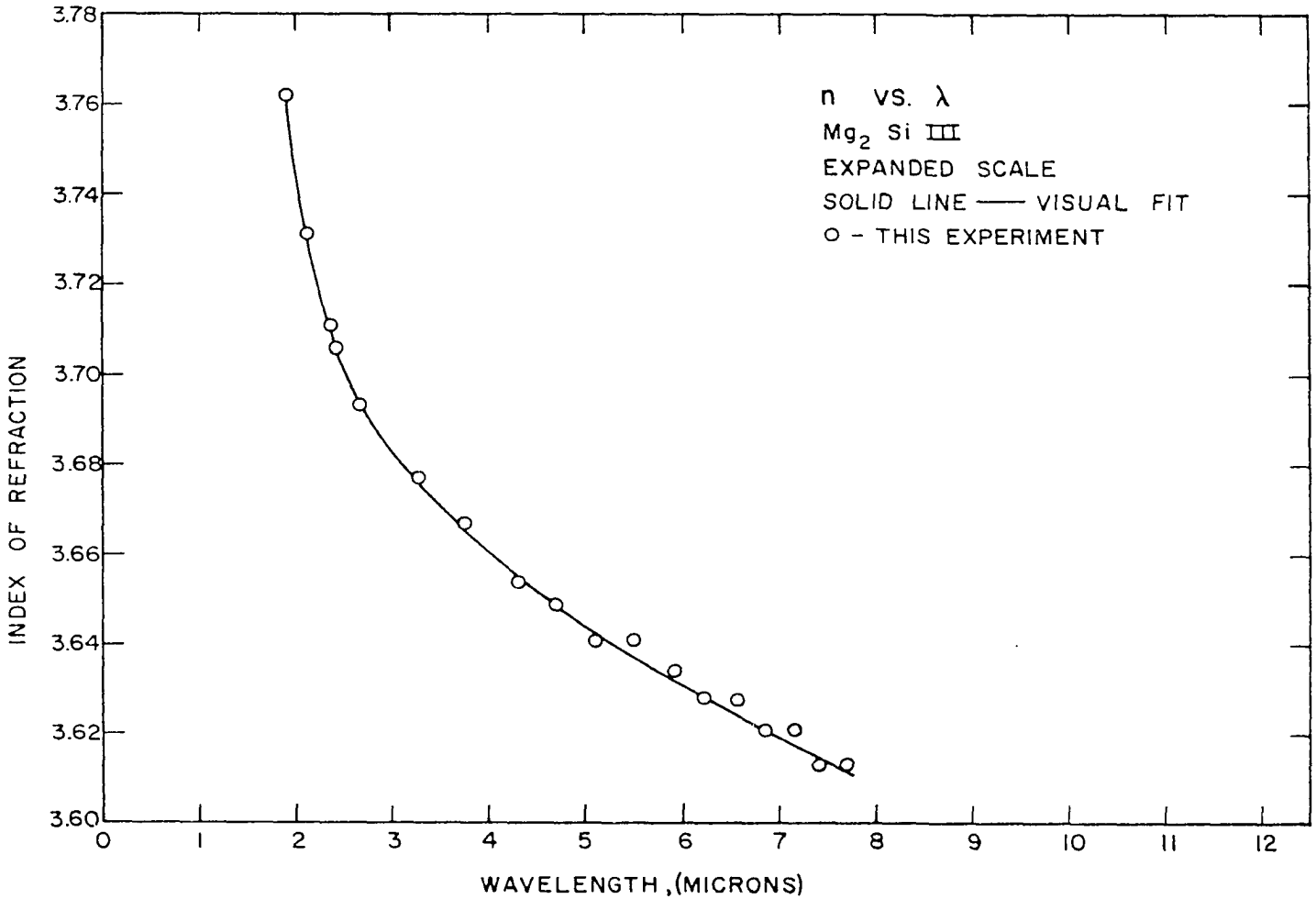

Figure 6. Index of refraction versus wavelength for Mg_2Si III prism

Table 1. Refractive index of Mg_2Si III

Wavelength (microns)	Index of refraction
1.90 ± 0.01	3.76 ± 0.01
2.10 ± 0.01	3.73 ± 0.01
2.35 ± 0.01	3.71 ± 0.01
2.40 ± 0.01	3.71 ± 0.01
2.65 ± 0.01	3.69 ± 0.01
3.25 ± 0.01	3.68 ± 0.01
3.77 ± 0.01	3.68 ± 0.01
4.26 ± 0.01	3.65 ± 0.01
4.70 ± 0.01	3.65 ± 0.01
5.12 ± 0.01	3.64 ± 0.01
5.52 ± 0.01	3.64 ± 0.01
5.90 ± 0.01	3.63 ± 0.01
6.23 ± 0.01	3.63 ± 0.01
6.55 ± 0.01	3.63 ± 0.01
6.86 ± 0.01	3.62 ± 0.01
7.16 ± 0.01	3.62 ± 0.01
7.45 ± 0.01	3.61 ± 0.01
7.72 ± 0.01	3.61 ± 0.01
9.00 ± 0.01	3.58 ± 0.06
10.60 ± 0.01	3.63 _ 0.02

indication of the data scatter in a restricted region of 1-8 microns. Several other Mg_2Si prisms gave the same results.

Figure 7 similarly shows a plot of the values for Mg_2Ge I given in Table 2. Here different prisms have been plotted with the precision indicated at each datum point. Where no error bar appears in the previous figures, the size of the data circle indicates the error of the determination, except for Figure 6.

All the available Mg_2Sn was highly absorbing and therefore required wide slits in order to make any determination

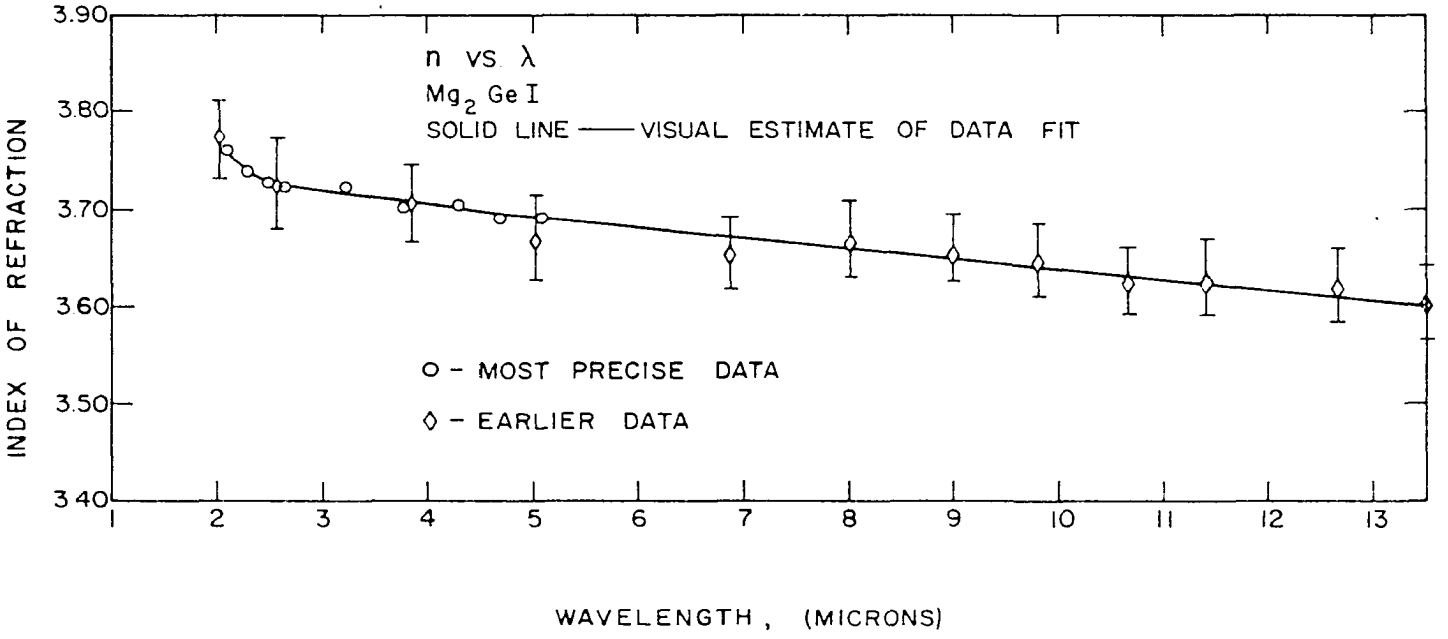

Figure 7. Index of refraction versus wavelength for Mg_2Ge I prism

Table 2. Refractive index of Mg_2Ge I

Wavelength (microns)	Index of refraction
2.10 ± 0.01	3.76 ± 0.01
2.35 ± 0.01	3.74 ± 0.01
2.40 ± 0.01	3.73 ± 0.01
2.40 ± 0.01	3.72 ± 0.01
2.65 ± 0.01	3.72 ± 0.01
3.25 ± 0.01	3.72 ± 0.01
3.77 ± 0.01	3.70 ± 0.01
4.26 ± 0.01	3.70 ± 0.01
4.70 ± 0.01	3.69 ± 0.01
5.12 ± 0.01	3.69 ± 0.01

at all. However, at the point of maximum transmission, approximately 5.2 microns, one measurement was made with a reasonably small error. This single value, combined with the data obtained with wider slits and the observation that widening the slits lowers the measured value of the index of refraction, led to the solid line plotted in Figure 8. These data are given in Table 3. The Mg_2Sn was obtained from H. Guennoc of the Compagnie generale de. T.S.F., Paris, France.

Figure 9 is a summary of the data presented thus far.

The possible errors indicated in Tables 1, 2 and 3 are based on experimental observations of the values obtained for Si for different slit widths and the fact that the small sample prisms did not have perfectly flat faces. The lack of flatness was detectable in the determination of the apex

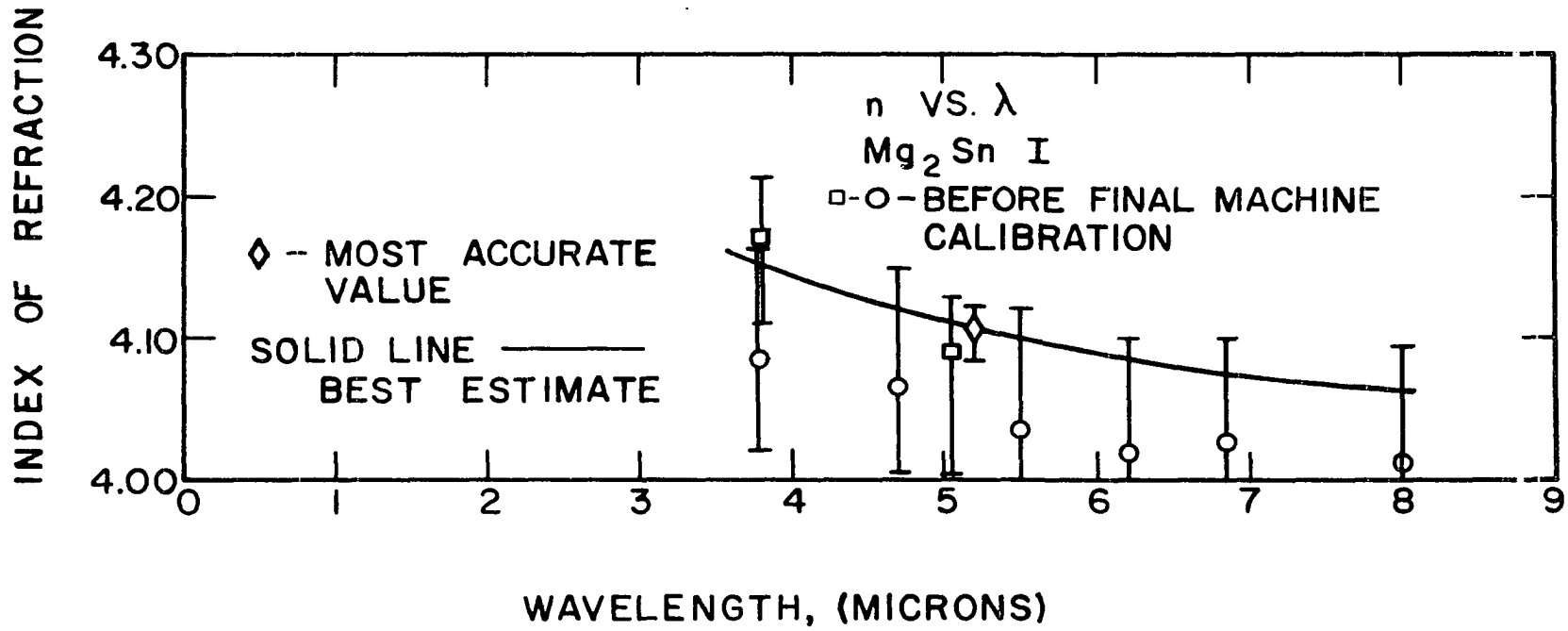

Figure 8. Index of refraction versus wavelength for Mg_2Sn I prism

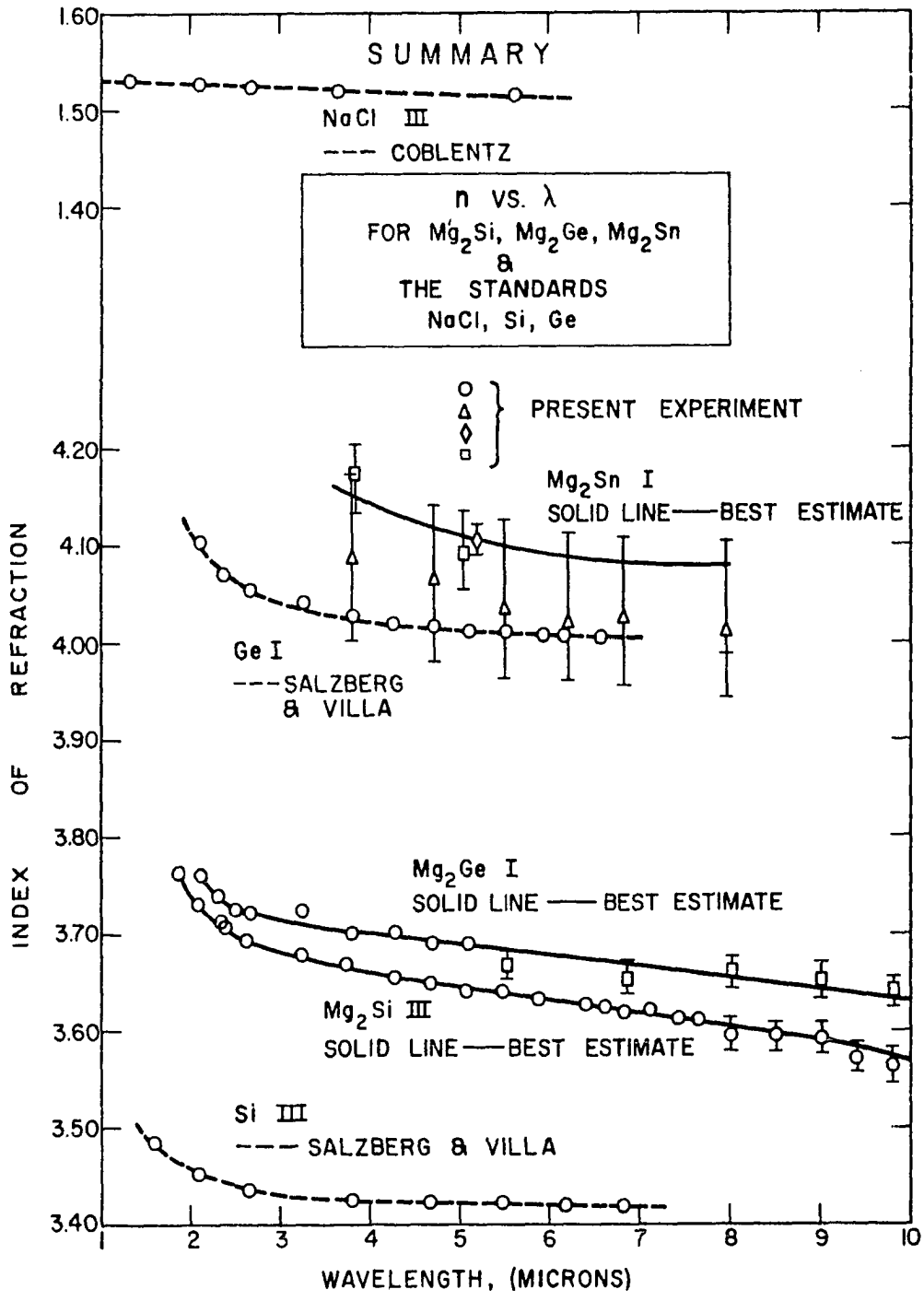

Figure 9. Summary of index of refraction measurements

Table 3. Refractive index of Mg_2Sn I

Wavelength (microns)	Index of refraction
Slit 0.1 mm	
5.20 ± 0.01	4.11 ± 0.02
Slit 0.5 mm	
3.77 ± 0.01	4.07 ± 0.07
4.70 ± 0.01	4.07 ± 0.07
5.52 ± 0.01	4.07 ± 0.07
6.23 ± 0.01	4.02 ± 0.07
6.86 ± 0.01	4.03 ± 0.07
8.00 ± 0.01	4.01 ± 0.07
3.77 ± 0.01	4.09 ± 0.07
Slit 0.3 mm	
3.77 ± 0.01	3.61 ± 0.03
5.05 ± 0.01	3.57 ± 0.03

angle. The slit image in these cases was broadened by the surface curvature of the prism face. The outside edges of the image were used to determine the range of possible values of the apex angle. In all cases this range was less than 1 minute of angle. The wavelength errors could have been easily reduced with more careful monochromator calibration. However, this did not seem necessary when the large possible error in the index of refraction measurement was considered.

III. MEASUREMENT OF REFLECTIVITY

Shown in Figure 10 is the optical arrangement used to determine the reflectivity of Mg_2Si, Mg_2Sn and Mg_2Ge in the infrared. Light from the Globar passed through a 13 cycles-per-second chopper and was focused by the mirror M_1 on the sample, S, at near normal incidence. The angle of incidence was approximately 12°. Reflected light from the sample was then focused by the mirror M_2 on the entrance slit of a prism monochromator. This monochromator employed a NaCl prism for the wavelength range from 2 microns to 16 microns, a KBr prism for the wavelength range from 5 microns to 21 microns and a CsI prism for the wavelength range of 20 microns to 50 microns. The light exiting from the prism monochromator entered the grating monochromator used for wavelength calibration. After prism calibration, the grating was replaced with a plane mirror, M_4, which reflected light directly back to the collimating mirror, M_5, without dispersion. The beam was then focused by M_8 on a Reeder thermocouple detector with a CsI window.

The mirror, M_7, could be replaced by a scatter plate or a reststrahlen reflection filter. In addition, a transmission filter of polyethylene sanded on both sides could be introduced into the beam at the entrance slit of the grating monochromator. Various combinations of filters and reflection

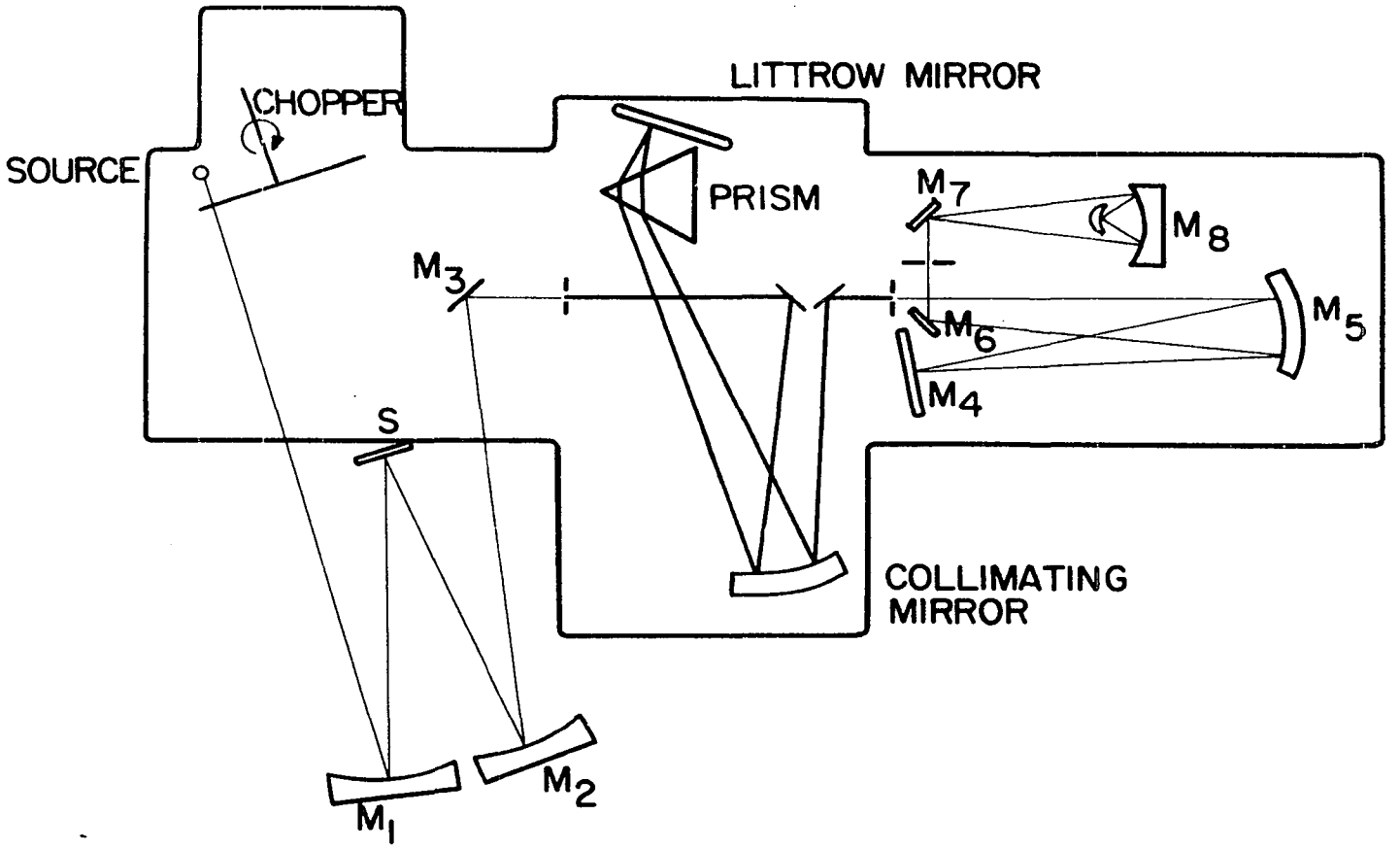

REFLECTIVITY APPARATUS

Figure 10. Apparatus for the reflectivity determination

filters were used to reduce unwanted radiation at the detector. Table 4 lists the wavelength ranges, prisms and various filtering techniques with the filter used to estimate the stray light contribution.

An electric motor and transmission were utilized to drive the prism Littrow mirror through the desired wavelength ranges. The detection and recording equipment were as previously described, with the output voltage continuously indicated on a strip chart.

The reflectivity was determined by comparing the output voltage with the sample in place with that obtained by reflection from Al at the sample position. A typical measurement in the 40 micron to 47 micron region began with the measurement of the signal obtained from Al at the sample position, followed by the measurement of the signal with an opaque filter in front of the entrance slit. Next a measurement was made of the signal with a NaCl window 6.5 millimeters thick in front of the entrance slit. The NaCl window did not transmit any light with wavelength longer than 23 microns, but transmitted a large fraction of all light with wavelength less than 20 microns. The sample was positioned in place of the Al and a determination made of the signal with and without the NaCl window before the entrance slit. Throughout these determinations the two thicknesses of polyethylene remained in the optical path. The NaCl window

Table 4. Wavelength ranges, prisms and filtering techniques

Wavelength (microns)	Prism	Filter	Filter for stray light determination	Stray light	Correction applied to zero
2 - 5	NaCl	None	None	Less than 0.1% (estimated)	No
5 - 10	NaCl	None	Glass 1 mm thick	Less than 0.5%	No
10 - 15	NaCl	Scatter plate	Fused SiO_2 1 mm thick	Less than 1.0%	No
8 - 15	KBr	Scatter plate	Fused SiO_2 1 mm thick	Less than 1.0%	No
15 - 20	KBr	Scatter plate	CaF_2 5 mm thick	Less than 1.0%	No
20 - 30	CsI	Two thicknesses polyethylene sanded both sides	CaF_2 5 mm thick	Less than 1.0%	No
30 - 40	CsI	Two thicknesses polyethylene sanded both sides	NaCl 6.5 mm thick	Less than 5.0%	Yes
40 - 47	CsI	Two thicknesses polyethylene sanded both sides	KBr 6.5 mm thick	Less than 25.0%	Yes
47 - 54	CsI	Two thicknesses polyethylene sanded both sides	KBr 6.5 mm thick	Less than 50.0%	Yes

transmission was measured between 2.5 microns and 15 microns with a Beckman IR-7 monochromator. The transmission was close to 0.88 for the entire range. In order to correct for the stray light reflection by the NaCl window, all readings with the window in place were multiplied by 1.14. This value was subtracted from the readings without the window in place for both the sample and Al. The ratio of these two differences was recorded as the reflectivity. Where the stray light was small, no correction was needed. The alignment of the beam was done visually and was optimized for each run. The entire monochromator, sample and source volumes were swept with dry N_2.

Figure 11 shows the reflectivity obtained from a freshly cleaved NaCl surface. Also pictured is the reflectivity of NaCl as determined by Mitsuishi *et al.* (17). The monochromator was operated in this range with 2 millimeter slits, which may be the reason the two humps on the left were not observed.

The reflectivity of a cleaved Mg_2Si surface was compared with the reflectivity of the same surface after light polishing with Al_2O_3 on a nap cloth. The great differences in reflectivity led to the use of cleaved surfaces for the rest of the observations. In some cases, however, the samples were not perfect cleavage surfaces. There were many steps in the cleaved surface for some of the determinations.

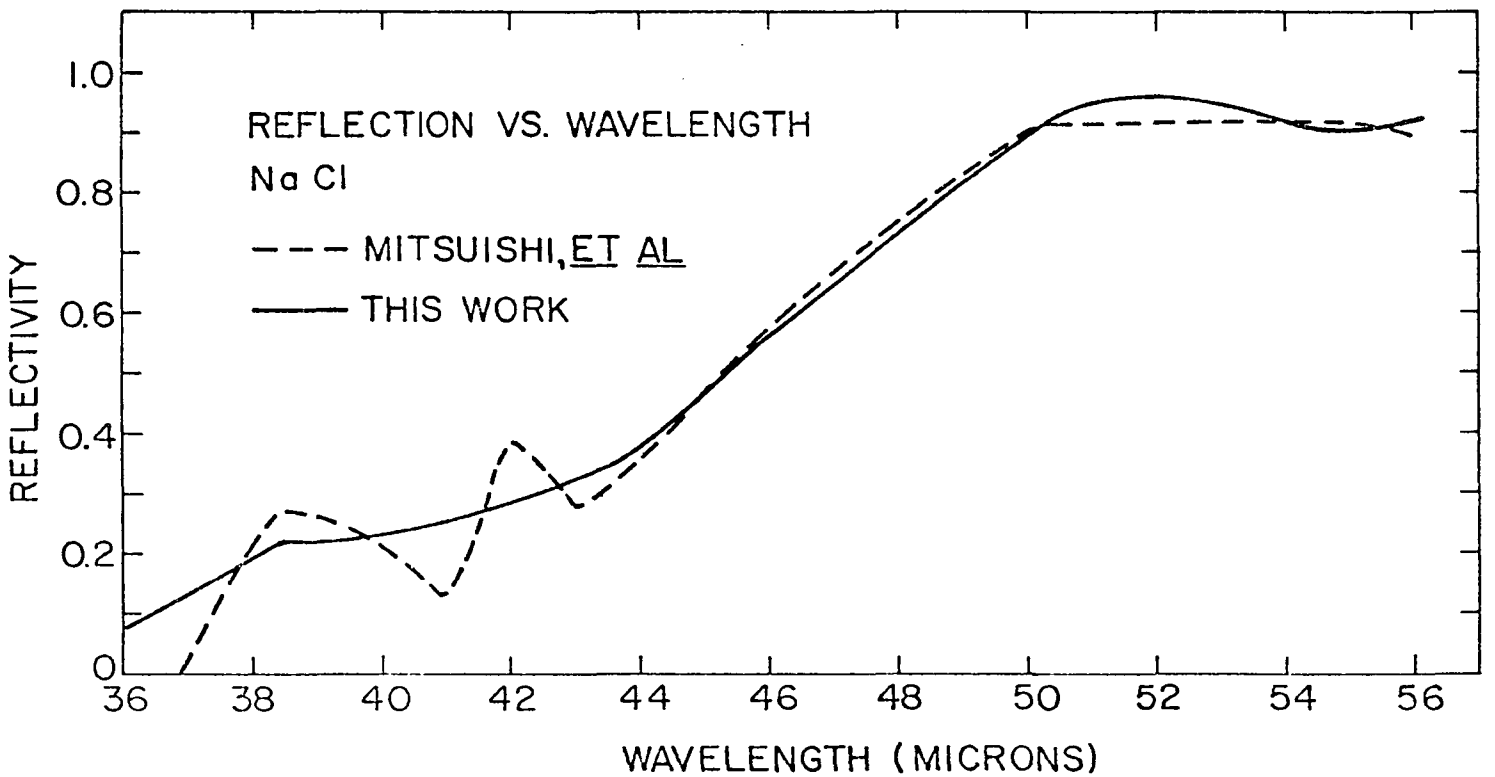

Figure 11. Reflectivity of NaCl

The faces of the steps were mostly parallel. It is believed that all samples used had reflectivities within 5 per cent of that which might have been obtained from a perfect face. All samples utilized in this experiment had been aged in air for a period of not less than thirty days. A surface film on the samples of Mg_2Si and Mg_2Ge was visually detectable, although slight. The sample of Mg_2Sn obtained from H. Guennoc was covered with a more obvious surface film.

IV. REFLECTIVITY RESULTS

The reflectivity obtained from a cleaved Mg_2Si surface is shown in Figure 12. The three x's on the left of the figure are reflectivities calculated from the index of refraction. The two datum points above the curve at 20 microns were not reproduced in subsequent determinations and are discounted. Figure 13 shows the reflectivity obtained from four samples of Mg_2Ge, three of which were doped with Al and Ag to yield the indicated carrier concentration determined by L. Lott from Hall data at room temperature. Figure 14 shows the reflectivity obtained for Mg_2Sn. Beyond 45 microns the CsI prism yielded a very small signal. As can be seen in Figure 12, where the actual datum points are included, the reflectivity beyond 45 microns is not precisely known. The small bump in Figure 14 falls in this region of uncertainty.

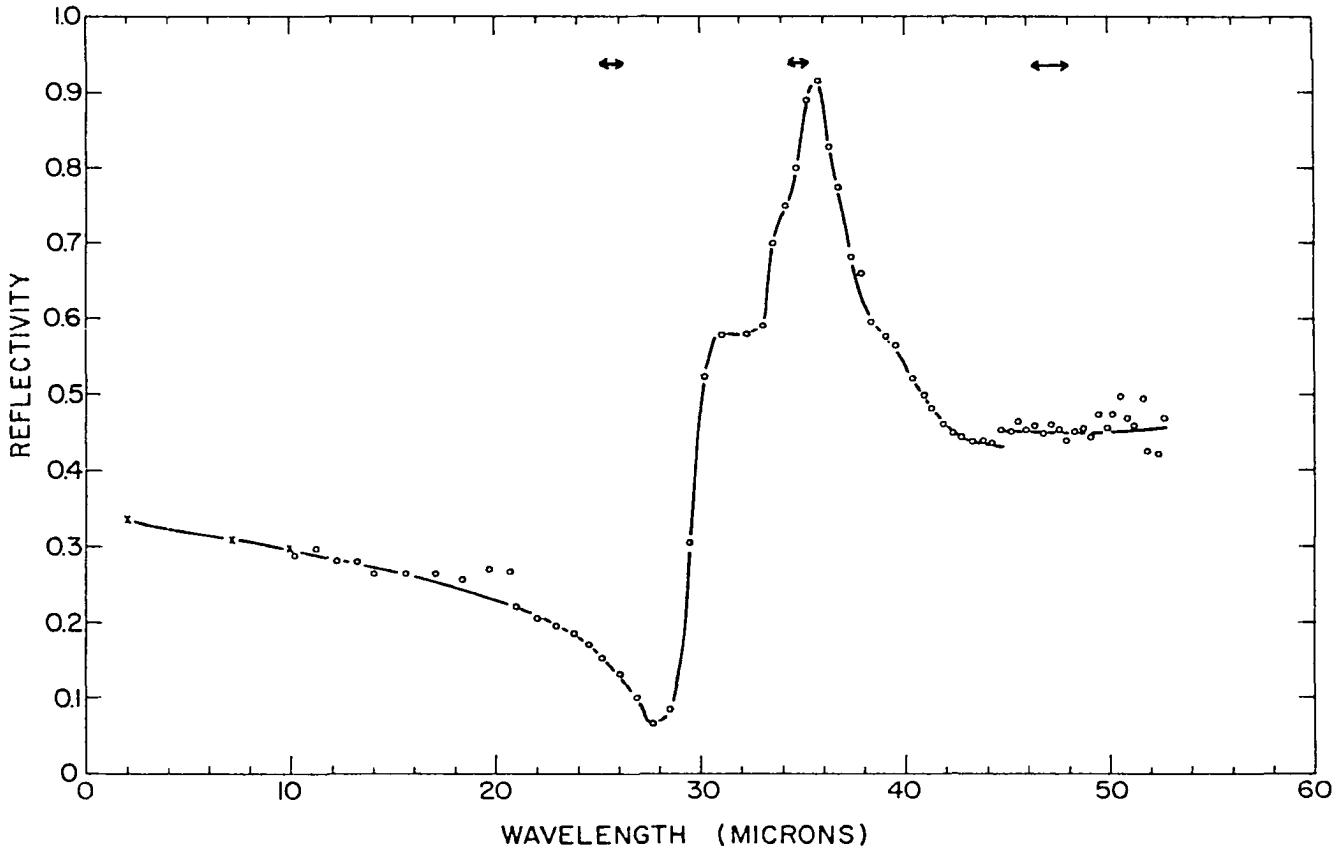

Figure 12. Reflectivity of Mg_2Si. (The arrows indicate the band width of the monochromator. $N = -1.0 \times 10^{23}$ per cubic meter)

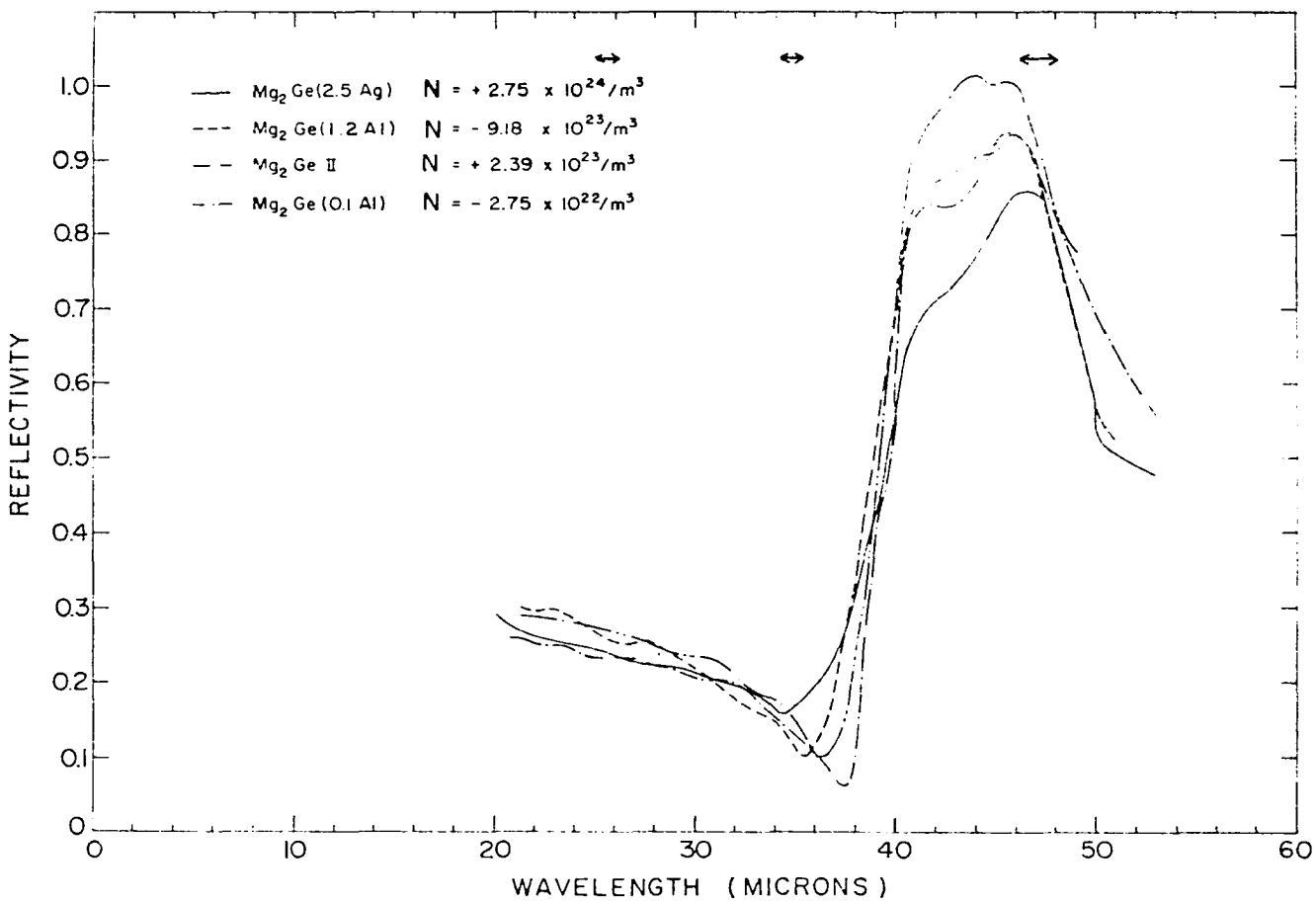

Figure 13. Reflectivity of Mg_2Ge. (The arrows indicate the band width of the monochromator)

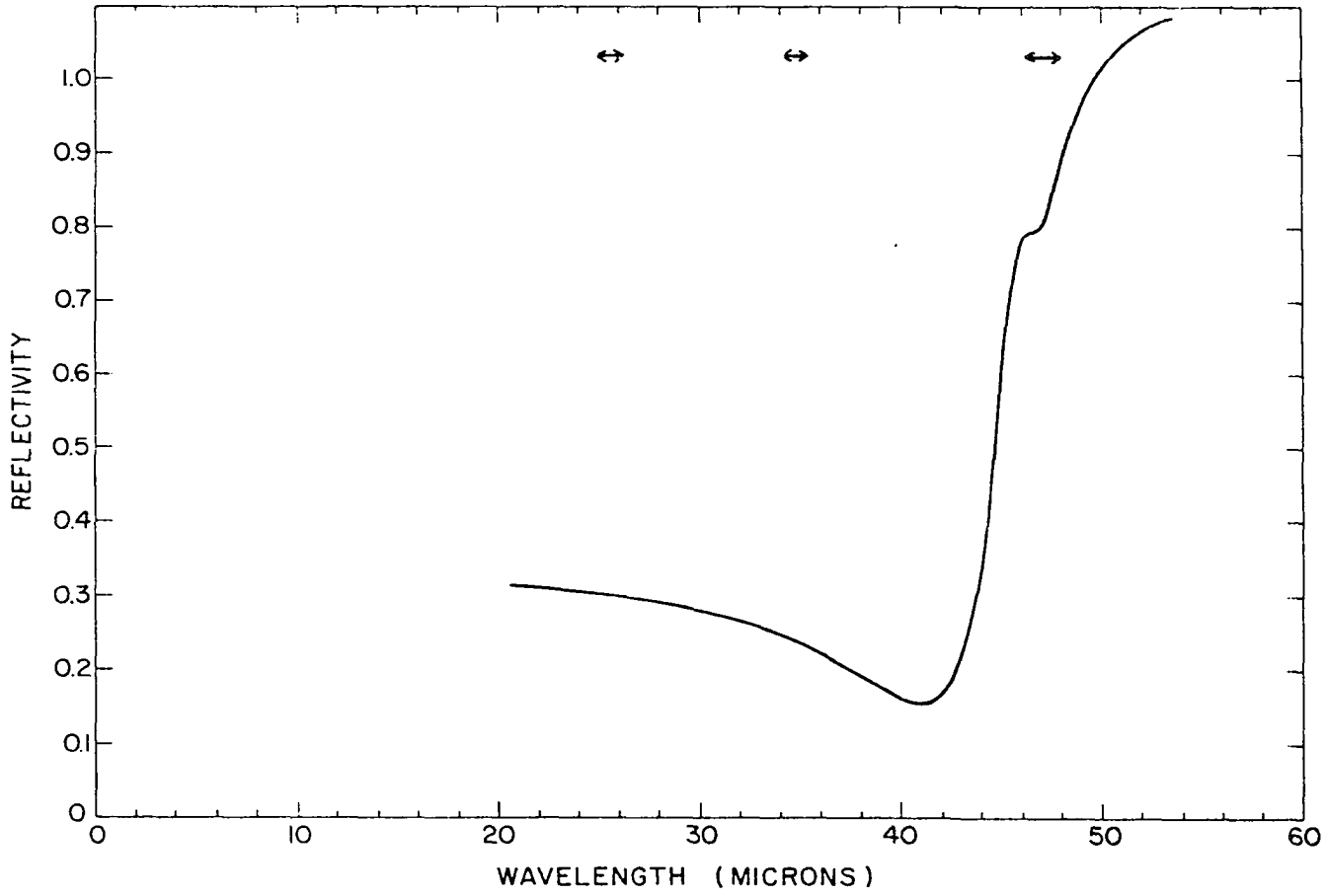

Figure 14. Reflectivity of Mg_2Sn with different carrier concentrations. (The arrows indicate the band width of the monochromator. $N = -3.0 \times 10^{24}$ per cubic meter)

V. DISCUSSION

Figure 15 shows the reflectivity of Mg_2Si II compared with the reflectivity of a classical oscillator as described in Appendix B. The classical oscillator curve shown in Figure 15 typifies the type of curve which can be said to approximate the data. This curve was one with $\rho = 0.63$, $\gamma = 0.01$, $\nu_o = 8.00 \times 10^{12}$ per second, and $\epsilon = 12$. Figure 16 shows another plot with different values of the parameters, ρ, γ and ϵ. ν_o is the reststrahlen frequency, γ is called the strength of the oscillator, ρ is the width of the oscillator and ϵ is the short wavelength limiting value of the dielectric constant (see Appendix B).

Figure 17 is a classical oscillator approximation for Mg_2Ge reflectivity with $\rho = 0.5$, $\gamma = 0.007$, $\nu_o = 6.2 \times 10^{12}$ per second and $\epsilon = 14$.

The lack of a long wavelength limiting value of the reflectivity makes it difficult to fit a classical oscillator to the Mg_2Ge data with any confidence in the values of ρ, γ and ϵ. ν_o, however, should be quite close to the real value. If the same curve shape is assumed for Mg_2Sn, an approximate value for ν_o would be 5.6×10^{12} per second.

Ganesan and Srinivasan (18) have examined the three dimensional CaF_2 lattice to obtain a relationship

$$\mu \omega_r^2 = f$$

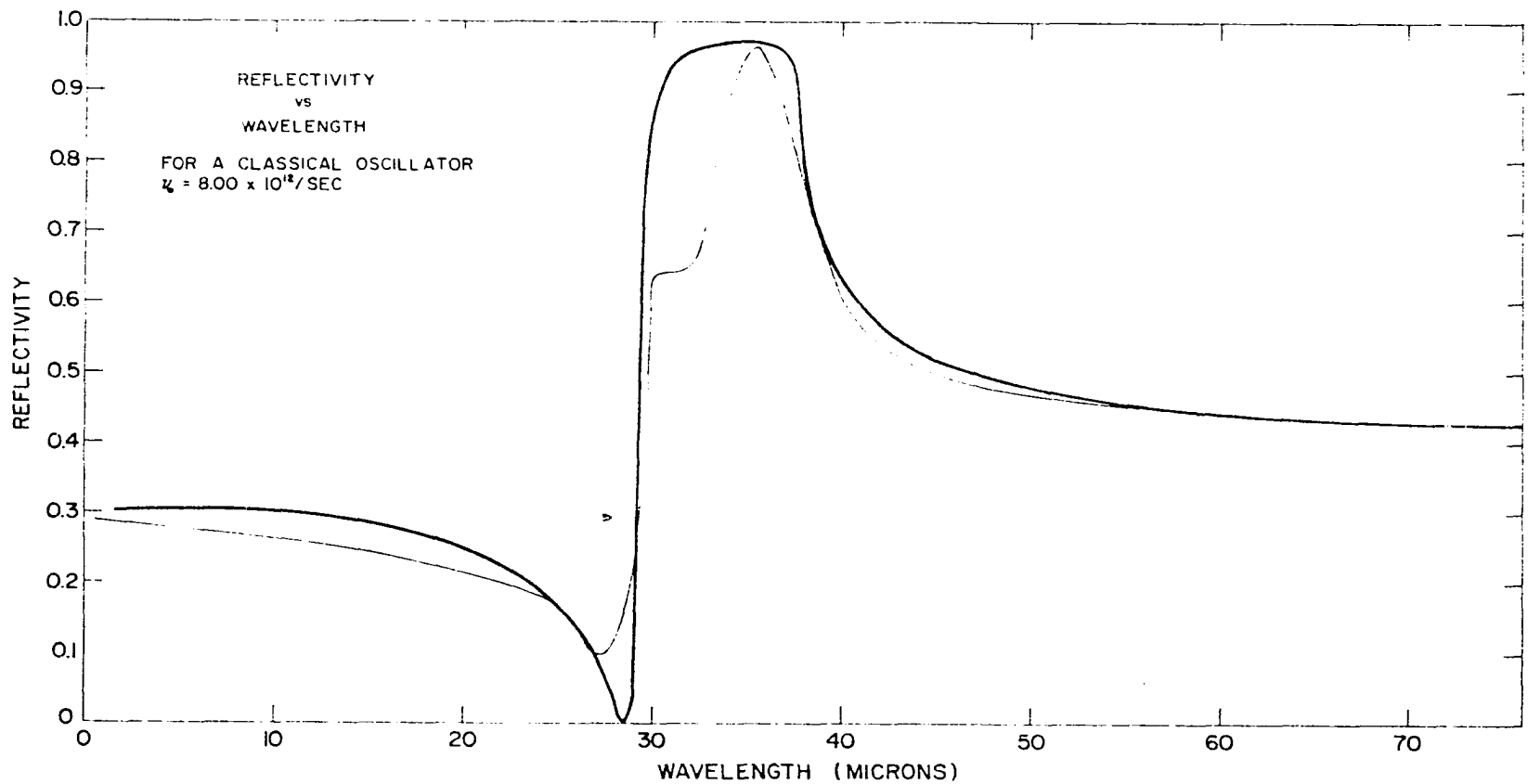

Figure 15. Reflectivity of a classical oscillator (dark line) compared to the reflectivity of Mg_2Si II. ($\nu_o = 8 \times 10^{12}(\text{seconds})^{-1}$, $\rho = 0.63$, $\gamma = 0.01$ and $\epsilon = 12$)

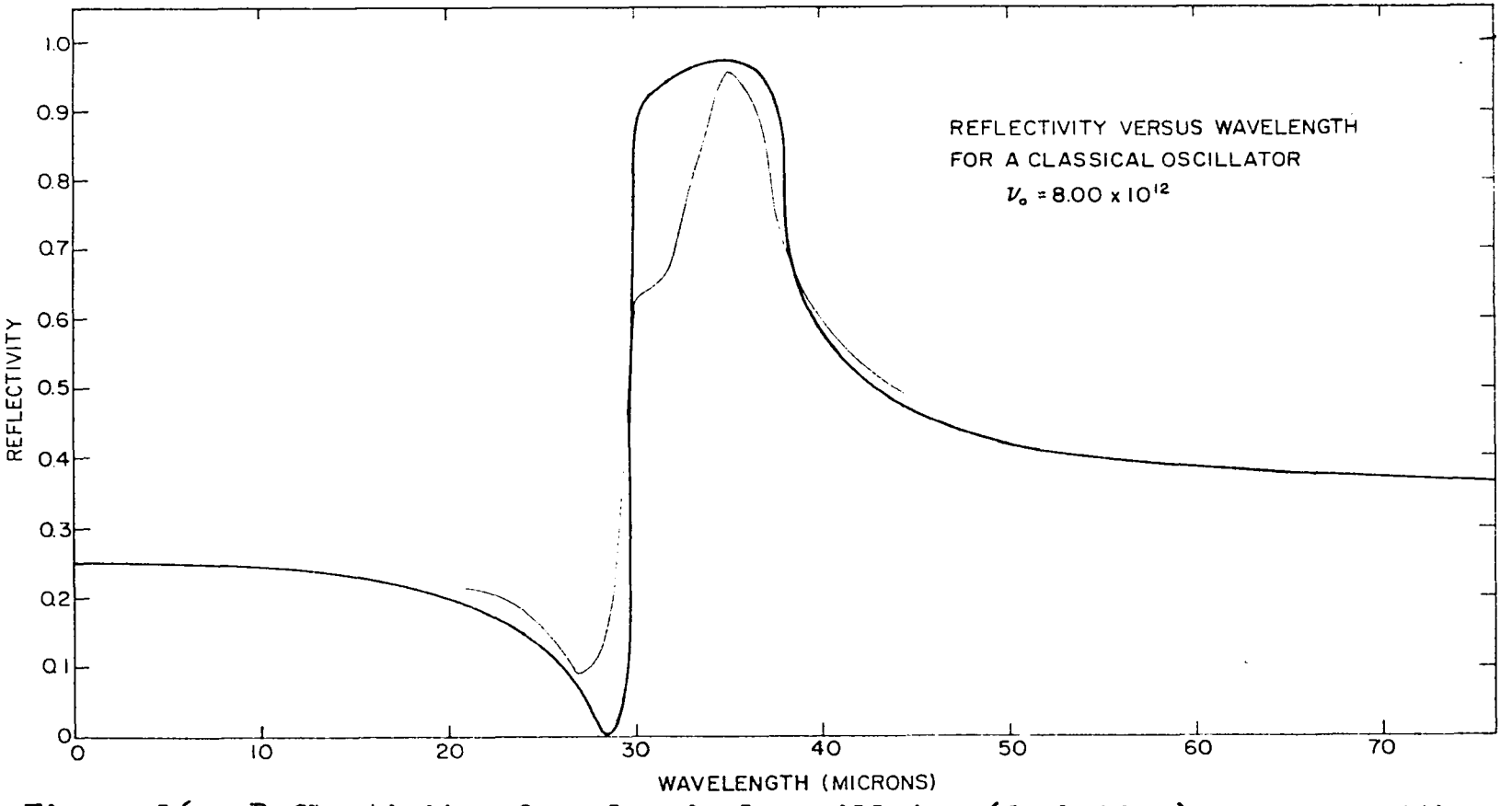

Figure 16. Reflectivity of a classical oscillator (dark line) compared with the reflectivity of Mg_2Si II. ($\gamma_o = 8 \times 10^{12}$ (second)$^{-1}$, $\rho = 0.45$, $\gamma = 0.01$ and $\epsilon = 9$)

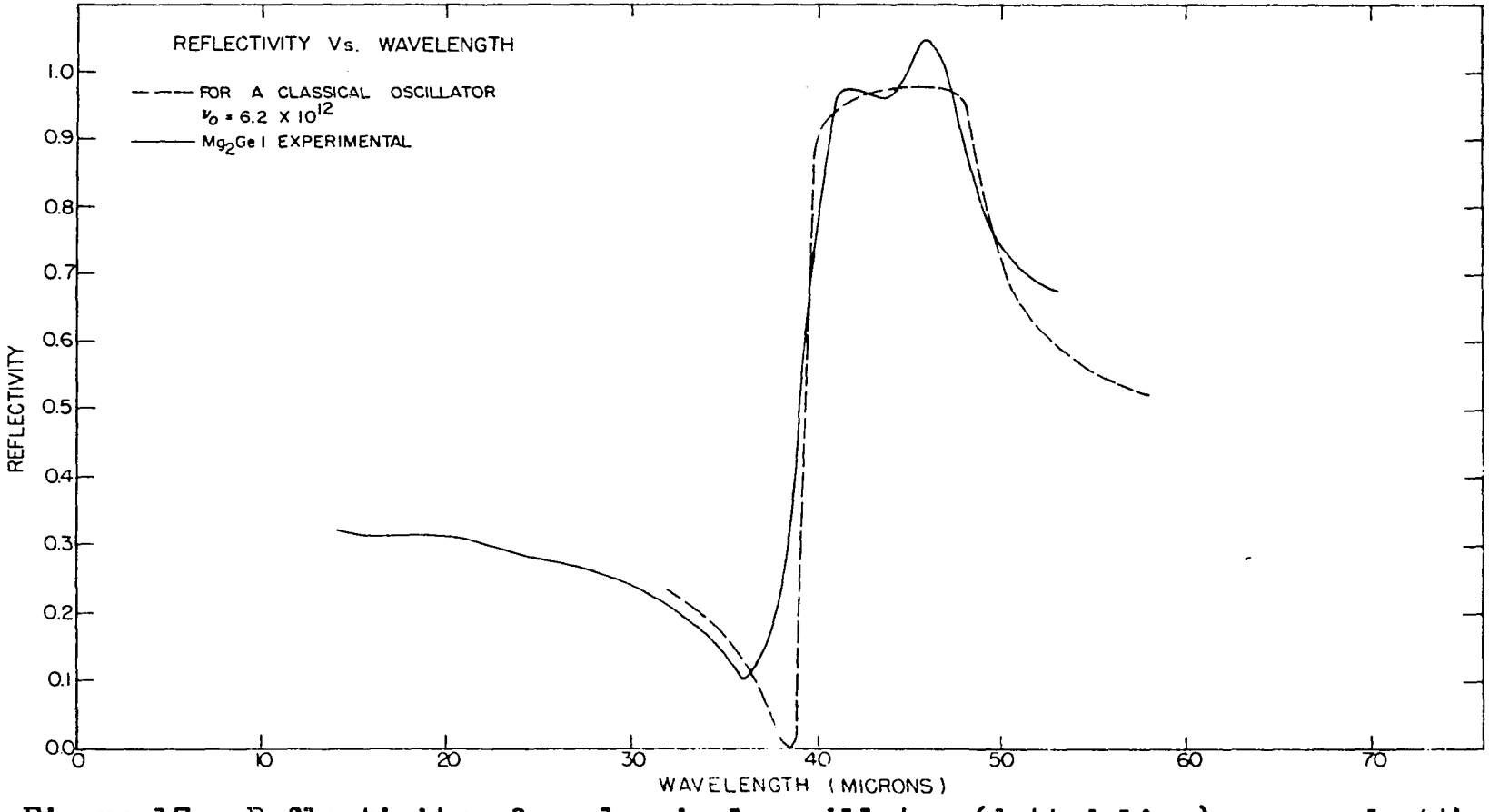

Figure 17. Reflectivity of a classical oscillator (dotted line) compared with the reflectivity of Mg_2Ge I. ($\gamma_0 = 6.2 \times 10^{12}(\text{second})^{-1}$, $\rho = 0.5$, $\gamma = 0.007$ and $\epsilon = 14$)

where μ is the reduced mass, ω_r is the reststrahlen frequency and f is a function including the Coulomb interaction and other terms pertaining to the lattice forces. Whitten (12) has made a similar solution for Mg_2Si. It is interesting to examine the ratios of the experimental reststrahlen frequencies as given by the classical oscillator approximations. For Mg_2Si

$$\mu_{Mg_2Si} = \frac{m_{Si}\, m_{Mg}}{m_{Si} + 2m_{Mg}} = 1.47 \times 10^{-26} \text{ kilograms}$$

and

$$\mu_{Mg_2Ge} = 2.42 \times 10^{-26} \text{ kilograms}$$

also

$$\mu_{Mg_2Sn} = 2.86 \times 10^{-26} \text{ kilograms.}$$

Now

$$\sqrt{\frac{\mu_{Mg_2Si}}{\mu_{Mg_2Ge}}} = 0.78 \qquad \text{and} \qquad \sqrt{\frac{\mu_{Mg_2Si}}{\mu_{Mg_2Sn}}} = 0.72 \ .$$

From the previous estimates

$$\frac{\omega_{r_{Mg_2Ge}}}{\omega_{r_{Mg_2Si}}} = 0.78 \qquad \text{and} \qquad \frac{\omega_{r_{Mg_2Sn}}}{\omega_{r_{Mg_2Si}}} = 0.70$$

which implies that f is a constant for the three materials.

An examination of Figure 13 reveals a small shift in the

reflectivity minimum as the carrier concentration changes. For a specific carrier sign the minimum shifts to shorter wavelengths as the concentration increases. Simultaneously the maximum value of the reflectivity decreases. The change in the reststrahlen reflectivity is very much like that observed by Yoshinaga and Oetjen (19) in their observations of the temperature dependence of the reflectivity for pure samples of InSb. Their lattice reflectivity changed with increasing temperature in the same fashion as the Mg_2Ge reflectivity changed with increasing carrier concentration.

It appears the changes in reflectivity are due to the free carriers and this is supported by an analysis suggested by Lynch[1].

The equations for the susceptibility and the conductivity were modified by a free carrier term [Moss (1, p. 29)] and written as

$$\chi = \chi_{co} - \frac{Ne^2\tau^2}{4\pi\varepsilon_o(1 + \omega^2\tau^2)m^*}$$

$$\sigma = \sigma_{co} + \frac{Ne^2\tau}{m^*(1 + \omega^2\tau^2)} .$$

---

[1]Lynch, D. W., Ames, Iowa. Influence of free carriers on the reflectivity of classical oscillators. Private communication. 1962.

The subscript co refers to the contribution of the classical oscillator as discussed in Appendix B. τ is the collision time of the free carriers.

Figure 18 shows the influence of classical free carriers on the classical oscillator according to these equations. Figure 18 (a) gives the experimental reflectivity for two Ag doped Mg_2Ge samples. Figure 18 (b) shows the classical oscillator without free carriers and with the addition of concentrations equal to the experimental concentrations for typical values of τ and m*/m. The similarities in these curves are offered as additional evidence that the gross changes of reflectivity in Mg_2Ge with doping are due to free carriers.

Many different combinations of ρ, γ, γ_o, ϵ, τ, and m*/m were substituted into the equations, and Figure 18 gives the curves which came closest to the experimental results. The value of τ which gave the best result is roughly in agreement with the collision time calculated from the resistivities reported by Redin (4) for Mg_2Ge. From his values a typical value for holes would be 2×10^{-14} seconds. Since the reflectivity measurements are a surface phenomenon, a shorter collision time would be expected. In the classical calculations reasonable results were obtained only for values of τ between 5×10^{-15} seconds and 10^{-14} seconds. When $\tau = 5 \times 10^{-15}$ seconds was used, m* = 0.2 m provided a result

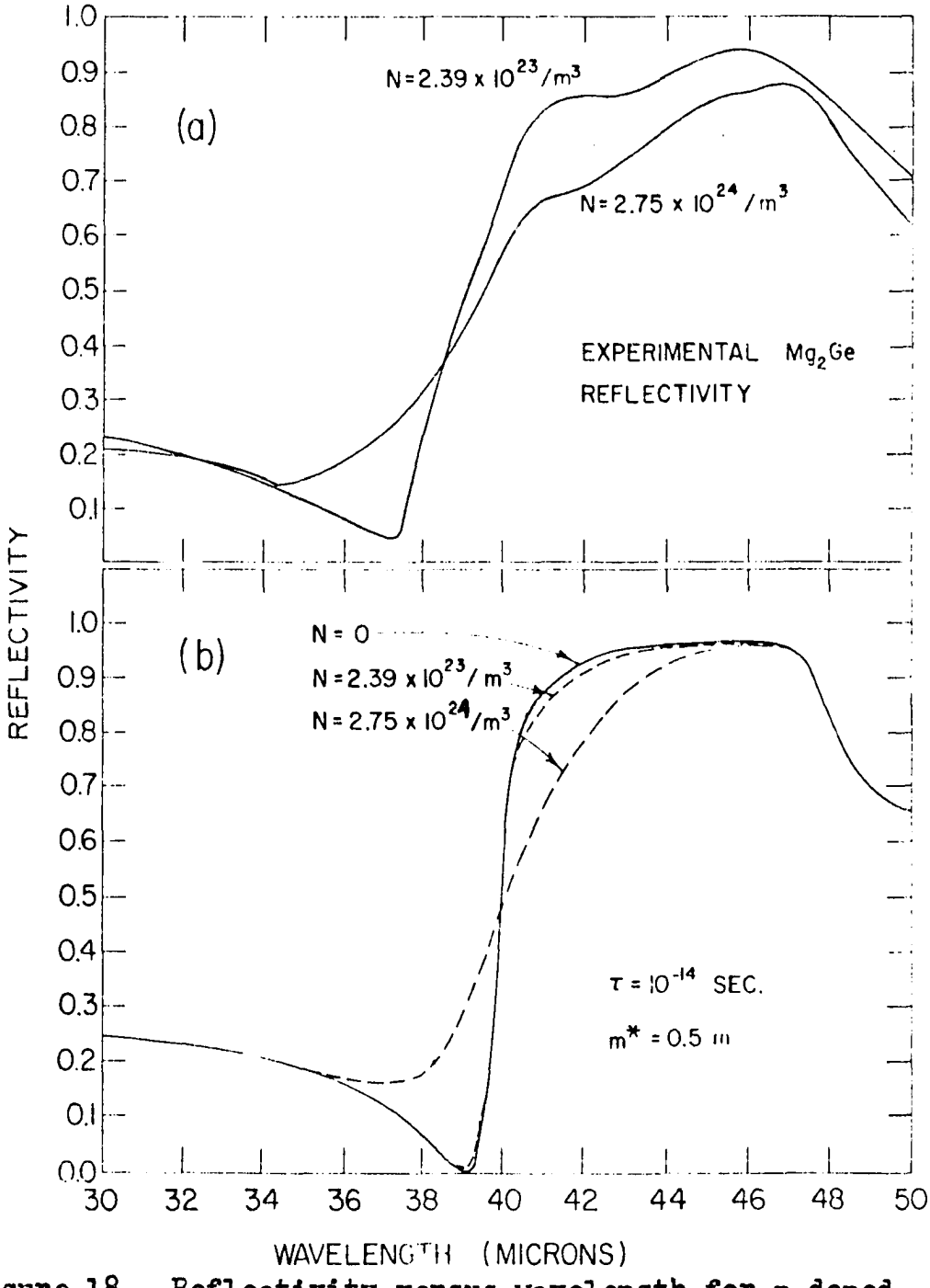

Figure 18. Reflectivity versus wavelength for p-doped Mg_2Ge and a classical oscillator with free carrier modifications

similar to that shown in Figure 18 (b). On a reasonability basis the conclusion that $m_h^* \geq 0.2$ seems proper.

The analysis for the Al doped samples was much less satisfactory. None of the combinations of constants tried gave results similar to the experiment. τ was varied from 10^{-16} seconds to 5×10^{-14} seconds. m*/m from 0.1 to 0.5 was tried. Both of these variations were matched with various values of ρ, γ, γ_o and ϵ. It was not possible to obtain a small shift in a sharp minimum when the minimum was required to be near zero. No explanation can yet be offered about the small effect of n doping on the Mg_2Ge reflectivity minimum.

Figure 19 shows the reflectivity data plotted against energy. The peak width decreases with increasing reduced mass. The decreasing width of the peak is similar to the observations of Lax and Burstein (20) on MgO, LiF, NaF, NaCl and KCl.

The cause of the bumps in the high reflectivity regions for these materials remains to be determined. There is a possibility that these bumps are due to multiple phonon effects as described by Lax and Burstein (20) and Kleinman (21) and observed by Turner and Reese (22) and others. Woods, et al. (23) have determined the energy-momentum relationships for phonons in KBr by neutron diffraction. With his values for energies of possible modes, one obtains several combina-

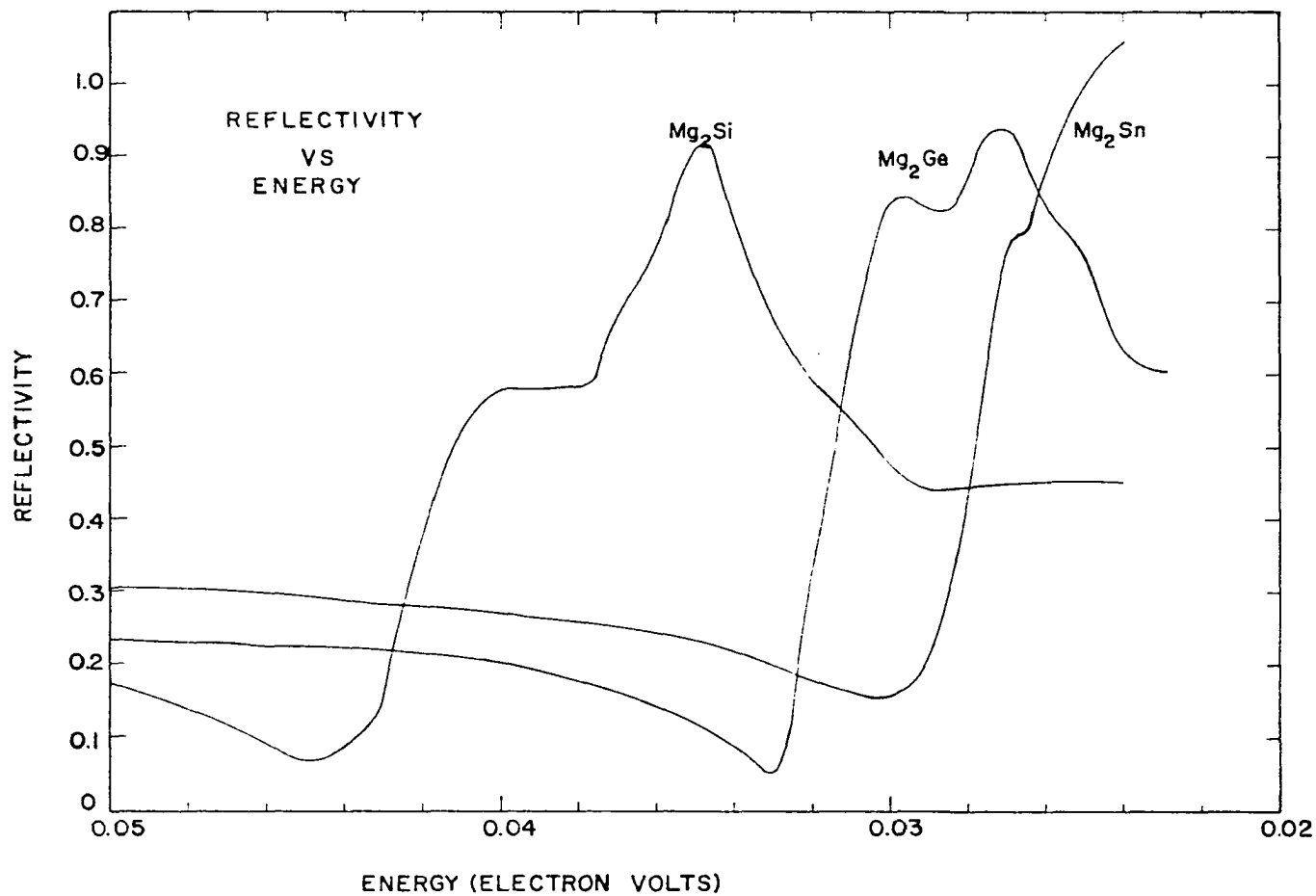

Figure 19. Reflectivity of the Mg compounds versus energy

tions of phonons which yield energies close enough together and at the correct wavelength to account for the small bump in the KBr reflectivity reported by Mitsuishi, et al. (17). The bumps observed in the Mg compound reflectivity are similar to those found in ionic crystals, particularly CaF_2 and BaF_2, but need further study before deciding on their origin. Bumps of this nature are not found in the III-V compounds [Picus, et al. (24)].

Most recent work confirming multiple phonon effects in semiconductors has its basis in large changes in the absorption constant with wavelength Turner and Reese (22) . The transmission of several Mg_2Si and Mg_2Ge crystals was examined between 1.5 microns and 40 microns. None of these determinations showed changes in transmission which could be attributed to multiple phonon effects.

Because of the uncertainty in the long-wavelength reflectivity, it is not possible to determine a very reliable value for the ionicity by examining the differences in the dielectric constant. Szigeti (25) has derived an expression relating the optical dielectric constant, the static dielectric constant and the ionicity by assuming classical crystal fields. This relation essentially is the same as that given in Appendix B between ρ and e*.

$$\rho = \frac{2Ne^{*2}}{16\pi^3 \epsilon_0 \mu \nu_0^2}\left[\frac{\epsilon_\infty + 2}{3}\right]^2$$

where N is the concentration of ion triplets and μ is the reduced mass. The unit volume is $V = \frac{a^3}{4}$. a, the lattice constant, is 6.338×10^{-10} meters [Whitsett (3)].

For Mg_2Si

$$\rho = 0.63$$

$$N = 1.57 \times 10^{28} \text{ per meter}^3$$

which gives $e^* = 0.35$ e.

This implies only that the ionicity exists, but is not very great.

VI. BIBLIOGRAPHY

1. Moss, T. S. Optical properties of semiconductors. London, Butterworths Scientific Publications. 1959.

2. Morris, R. G. Semiconducting properties of Mg_2Si. Unpublished Ph.D. thesis. Ames, Iowa, Library, Iowa State University of Science and Technology. 1957.

3. Whitsett, C. R. Electrical properties of magnesium silicide and magnesium germanide. Unpublished Ph.D. thesis. Ames, Iowa, Library, Iowa State University of Science and Technology. 1955.

4. Redin, R. D. Semiconducting properties of Mg_2Ge single crystals. Unpublished Ph.D. thesis. Ames, Iowa, Library, Iowa State University of Science and Technology. 1957.

5. Blunt, R. F., Frederikse, H. D. R. and Hosler, W. R. Electrical and optical properties of intermetallic compounds. IV. Magnesium stannide. Phys. Rev. 100: 663. 1955.

6. Koenig, P. J., Lynch, D. W. and Danielson, G. C. Infrared absorption in magnesium silicide and magnesium germanide. J. Phys. Chem. Solids 20: 122-126. 1961.

7. Winkler, V. Die elektrischen Eigenschaften der intermetallischen Verbindungen Mg_2Si, Mg_2Ge, Mg_2Sn, and Mg_2Pb. Helv. Phys. Acta 28: 617. 1955.

8. Heller, M. W. Seebeck effect in magnesium silicide. Unpublished Ph.D. thesis. Ames, Iowa, Library, Iowa State University of Science and Technology. 1960.

9. Moss, T. S. Photoconductivity of the elements. London, Butterworths Scientific Publications. 1952.

10. Madelung, O. H. Handbuch der Physik 20: 1. 1957.

11. Kittel, C. Introduction to solid state physics. 2nd ed. New York, N. Y., John Wiley and Sons, Ltd. 1957.

12. Whitten, W. Lattice vibrations of Mg_2Si. Unpublished paper. Typewritten. Ames, Iowa, Department of Physics, Iowa State University of Science and Technology. ca. 1962.

13. Fröhlich, H. Theory of dielectrics. London, Oxford University Press. 1949.

14. Ziman, J. M. Electrons and phonons. London, Oxford University Press. 1960.

15. Coblentz, W. W. Transmission and refraction data on standard lens and prism material with special reference to infra-red spectroradiometry. J. Opt. Soc. Am. 4: 432. 1920.

16. Salzberg, C. D. and Villa, J. J. Infrared refractive indexes of silicon germanium and modified selenium glass. J. Opt. Soc. Am. 47: 244. 1957.

17. Mitsuishi, A., Yamada, Y. and Yoshinaga, H. Reflection measurements on reststrahlen crystals in the far-infrared region. J. Opt. Soc. Am. 52: 14. 1962.

18. Ganesan, S. and Srinivasan, R. Lattice dynamics of calcium fluoride. I. Can. J. Phys. 40: 74. 1962.

19. Yoshinaga, H. and Oetjen, R. A. Optical properties of indium antimonide in the region from 20 to 200 microns. Phys. Rev. 101: 526. 1956.

20. Lax, M. and Burstein, E. Infrared lattice absorption in ionic and homopolar crystals. Phys. Rev. 97: 39. 1955.

21. Kleinman, D. A. Anharmonic forces in the GaP crystal. Phys. Rev. 118: 118. 1960.

22. Turner, W. J. and Reese, W. E. Infrared lattice bands in AlSb. Unpublished paper. Mimeographed. Yorktown Heights, New York, International Business Machines. 1962.

23. Woods, A. D. B., Brockhouse, B. N., Cochrane, W., Sakamoto, M. and Sinclair, R. N. Lattice vibrations of alkali halides. Bull. Am. Phys. Soc. Ser. 2, 5: 462. 1960.

24. Picus, G., Burstein, E., Henvis, B. W. and Hass, M. Infrared lattice vibration studies of polar character in compound semiconductors. J. Phys. Chem. Solids 8: 282. 1959.

25. Szigeti, B. Polarisability and dielectric constant of ionic crystals. Trans. Far. Soc. 45: 155. 1949.

26. Spitzer, W. G., Kleinman, D. and Walsh, D. Infrared properties of hexagonal silicon carbide. Phys. Rev. 113: 127. 1959.

27. Seitz, F. Modern theory of solids. New York, N. Y., McGraw-Hill Book Co., Inc. 1940.

VII. ACKNOWLEDGMENTS

The author is grateful for the many pertinent remarks and continual encouragement given by Dr. G. C. Danielson and Dr. D. W. Lynch. He also wishes to thank Mr. W. B. Whitten for many enlightening discussions.

VIII. APPENDIX A: LIST OF SYMBOLS

c = speed of light

E = electric intensity

E_o = amplitude of the electric intensity

f = a function of the lattice forces

$i = \sqrt{-1}$

$K = \frac{4\pi k}{\lambda}$ = absorption coefficient

k = imaginary part of the complex index of refraction called the extinction coefficient

m = mass of the electron

m_e^* = effective mass of electrons

m_h^* = effective mass of holes

N = magnitude of the carrier concentration

$\underline{N} = n - ik$ complex index of refraction

$\underline{N}^2 = n^2 - k^2 - 2 i n k$ = dielectric constant

n = real part of the complex index of refraction

R = reflectivity

t = time

x = displacement

α = angle of minimum deviation

γ = height of the resonance of a classical oscillator

δ = apex angle

ϵ = optical dielectric constant

ϵ_o = static dielectric constant

ϵ_0 = dielectric constant of free space

λ = wavelength of light

μ = reduced mass of a unit cell

ν_0 = reststrahlen frequency

π = 3.14159....

ρ = width of the resonance of a classical oscillator

σ = conductivity

σ_{co} = conductivity of a classical oscillator

τ = collision time of free carriers

χ = susceptibility

χ_{co} = susceptibility of a classical oscillator

ω = angular frequency

ω_r = reststrahlen angular frequency

ω_L = frequency of the longitudinal optical mode

IX. APPENDIX B: CLASSICAL OSCILLATOR EQUATIONS WITH FIGURES AND PRINTED COMPUTER SOLUTIONS

What follows is a quotation from the paper by Spitzer *et al.* (26) [CGS].

> According to the classical dispersion theory of crystals [Seitz (27)], the susceptibility χ and conductivity σ in the neighborhood of a resonance frequency ν_o are given by
>
> $$\chi = \rho \frac{1 - \nu^2}{(1-\nu^2)^2 + \gamma^2 \nu^2}, \qquad (1)$$
>
> and
>
> $$\frac{\sigma}{\nu} = 2\pi\rho \frac{\gamma\nu}{(1-\nu^2)^2 + \gamma^2 \nu^2}, \qquad (2)$$
>
> where ν is the measured frequency divided by ν_o, σ is the conductivity divided by ν_o, and the dimensionless parameters ρ and γ may be called the width and strength of the resonance, respectively. In the Lorentz theory, ρ is given by
>
> $$\rho = \frac{Ne^2}{4\pi^2 m^* \nu_o^2}, \qquad (3)$$
>
> where N is the concentration of ion pairs and m^* is their reduced mass. The index of refraction, n, and extinction coefficient, k, are given by
>
> $$n^2 = \frac{1}{2}\left\{\left[\epsilon^2 + 4(\sigma/\nu)^2\right]^{\frac{1}{2}} + \epsilon\right\}, \qquad (4)$$
>
> and
>
> $$k^2 = \frac{1}{2}\left\{\left[\epsilon^2 + 4(\sigma/\nu)^2\right]^{\frac{1}{2}} - \epsilon\right\}, \qquad (5)$$
>
> where
>
> $$\epsilon = \epsilon_o + 4\pi\chi, \qquad (6)$$
>
> and ϵ_o is the high-frequency ($\nu \gg 1$) dielectric constant.

According to Whitten (12) Equation 3 should read

$$\rho = \frac{2N_o^2}{4\pi^2 m^* \gamma_o^2} \qquad (7)$$

for the Mg compounds.

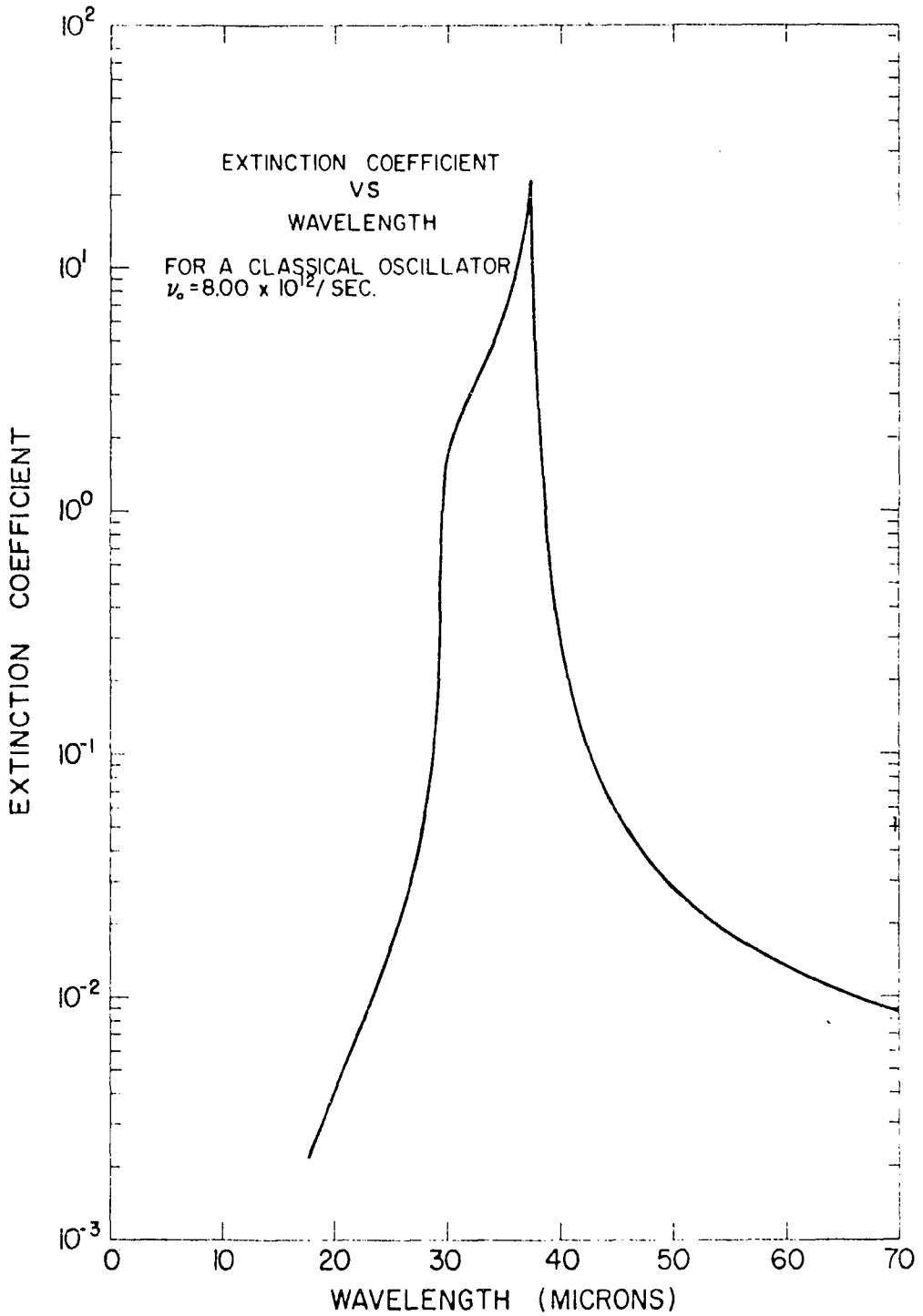

Figure 20. Extinction coefficient versus wavelength for a classical oscillator. $\gamma_o = 8 \times 10^{12}$ (seconds)$^{-1}$, $\rho = 0.63$, $\gamma = 0.01$ and $\epsilon = 12$

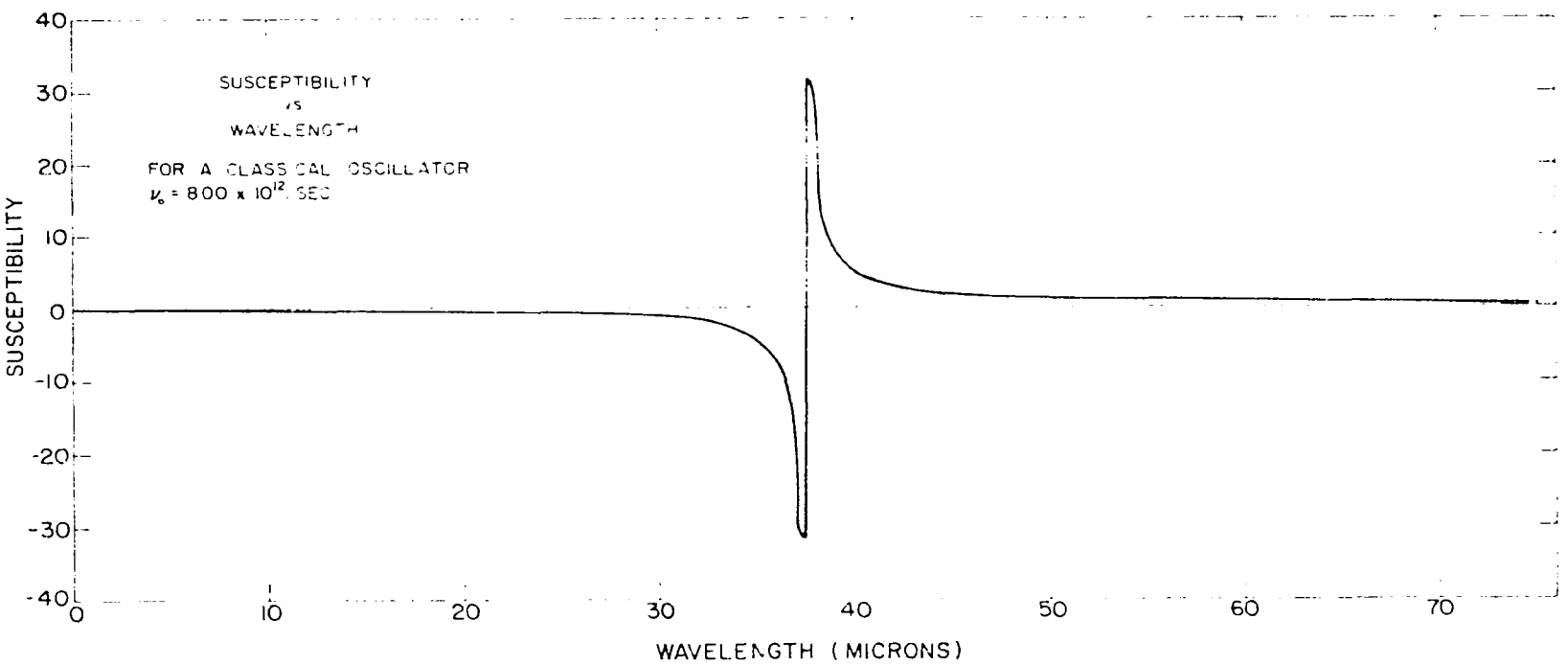

Figure 21. Susceptibility versus wavelength for a classical oscillator $\nu_o = 8 \times 10^{12}$ (seconds)$^{-1}$, $\rho = 0.63$, $\gamma = 0.01$ and $\epsilon = 12$

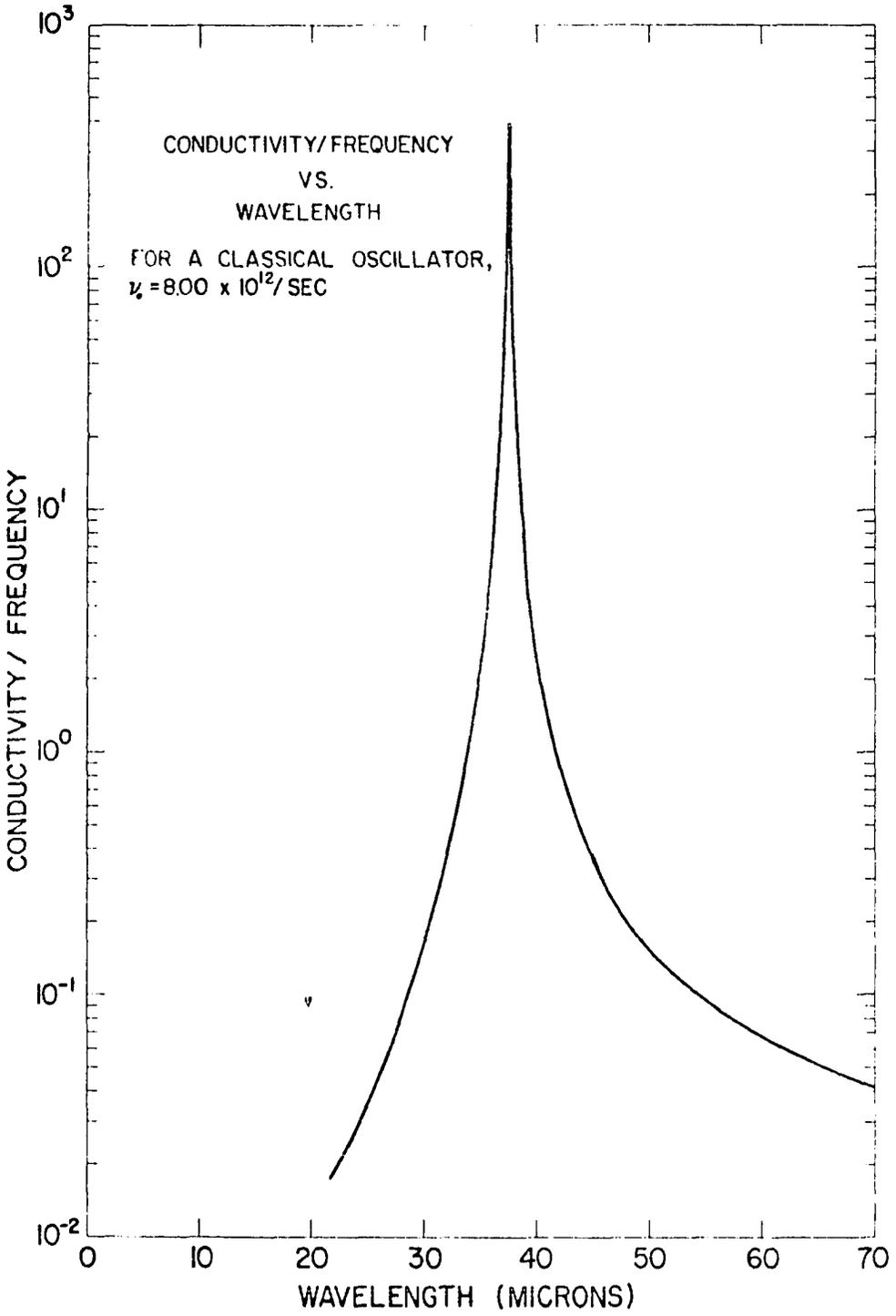

Figure 22. Conductivity/frequency versus wavelength for a classical oscillator. $\nu_o = 8 \times 10^{12}$ (seconds)$^{-1}$, $\rho = 0.63$, $\gamma = 0.01$ and $\epsilon = 12$

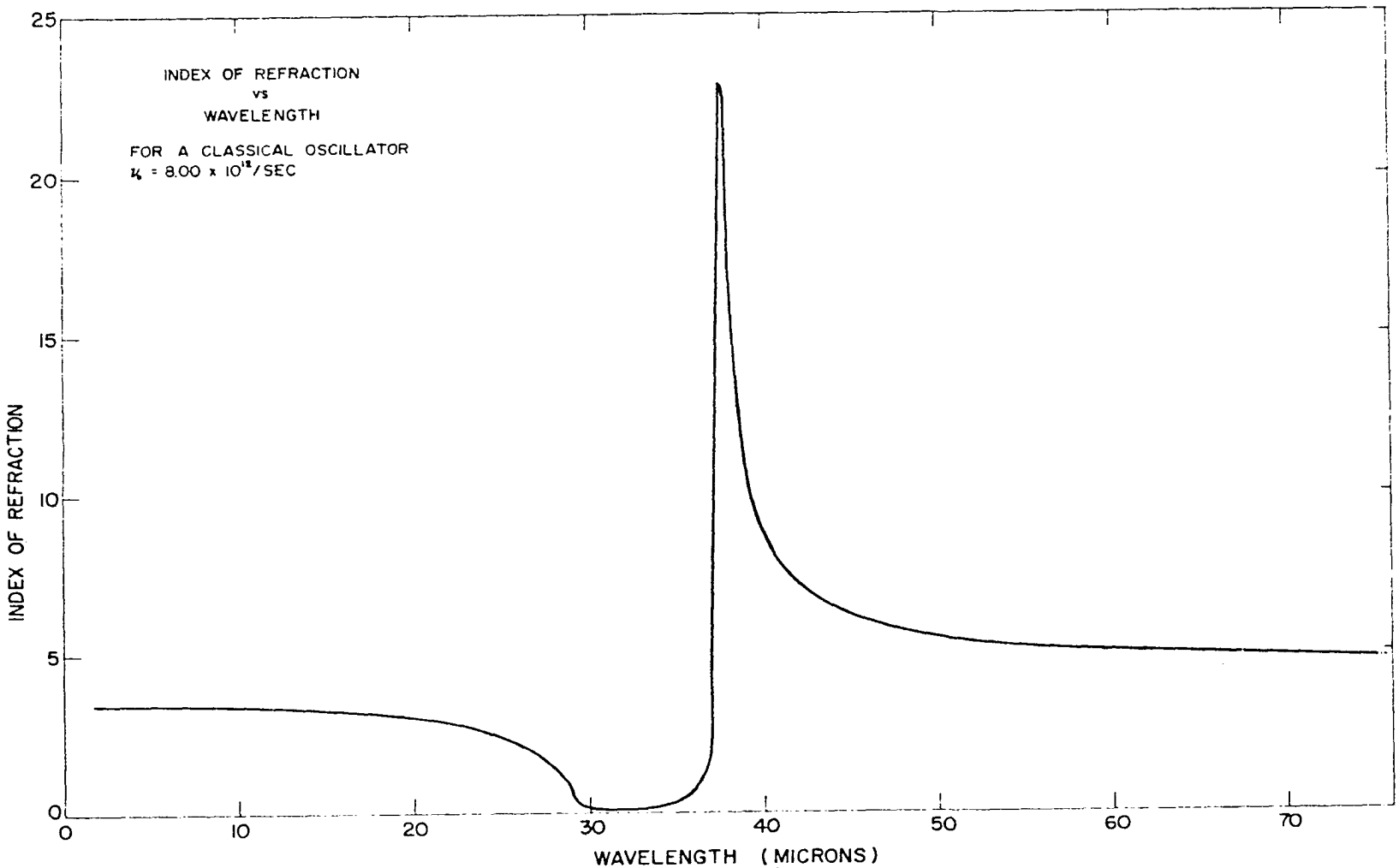

Figure 23. Index of refraction versus wavelength for a classical oscillator. $\gamma_0 = 8 \times 10^{12}$ (seconds)$^{-1}$, $\rho = 0.63$, $\gamma = 0.01$ and $\epsilon = 12$

Table 5. Computer solution for a classical oscillator

$\rho = 0.63$

$\gamma = 0.01$

$\gamma_0 = 8.00 \times 10^{12}$

$\epsilon = 12$

λ	χ	$\frac{\sigma}{\gamma}$	k	n	R
2.00×10^{0}	-1.80×10^{-3}	6.04×10^{-6}	2.11×10^{-4}	3.46×10^{0}	3.04×10^{-1}
6.00×10^{0}	-1.66×10^{-2}	1.71×10^{-4}	2.11×10^{-4}	3.43×10^{0}	3.01×10^{-1}
1.00×10^{1}	-4.82×10^{-2}	8.70×10^{-4}	2.11×10^{-4}	3.38×10^{0}	2.95×10^{-1}
1.40×10^{1}	-1.02×10^{-1}	2.78×10^{-3}	8.46×10^{-4}	3.27×10^{0}	2.83×10^{-1}
1.80×10^{1}	-1.89×10^{-1}	7.39×10^{-3}	2.38×10^{-3}	3.10×10^{0}	2.63×10^{-1}
2.20×10^{1}	-3.31×10^{-1}	1.86×10^{-2}	6.63×10^{-3}	2.80×10^{0}	2.25×10^{-1}
2.60×10^{1}	-5.83×10^{-1}	4.89×10^{-2}	2.26×10^{-2}	2.16×10^{0}	1.35×10^{-1}
3.00×10^{1}	-1.12×10^{0}	1.56×10^{-1}	1.44×10^{0}	1.08×10^{-1}	8.69×10^{-1}
3.40×10^{1}	-2.90×10^{0}	9.29×10^{-1}	4.95×10^{0}	1.88×10^{-1}	9.71×10^{-1}
3.80×10^{1}	2.11×10^{1}	5.00×10^{1}	2.96×10^{0}	1.69×10^{1}	7.95×10^{-1}
4.20×10^{1}	3.10×10^{0}	8.58×10^{-1}	1.20×10^{-1}	7.14×10^{0}	5.69×10^{-1}
4.60×10^{1}	1.88×10^{0}	2.87×10^{-1}	4.80×10^{-2}	5.97×10^{0}	5.08×10^{-1}
5.00×10^{1}	1.44×10^{0}	1.55×10^{-1}	2.83×10^{-2}	5.49×10^{0}	4.78×10^{-1}
5.40×10^{1}	1.22×10^{0}	1.03×10^{-1}	1.96×10^{-2}	5.22×10^{0}	4.61×10^{-1}
5.80×10^{1}	1.08×10^{0}	7.56×10^{-2}	1.49×10^{-2}	5.06×10^{0}	4.49×10^{-1}
6.20×10^{1}	9.93×10^{-1}	5.95×10^{-2}	1.20×10^{-2}	4.95×10^{0}	4.41×10^{-1}
1.10×10^{2}	7.13×10^{-1}	1.73×10^{-2}	3.77×10^{-3}	4.58×10^{0}	4.11×10^{-1}

X. APPENDIX C: INDEX OF REFRACTION DETERMINATION DATA

Table 6. Sextant calibration

Sextant setting	Sextant angle
42.5°	+ 19° 53'
40.0°	+ 17° 25.5'
37.5°	+ 14° 50'
35.0°	+ 12° 26'
32.5°	+ 9° 56'
30.0°	+ 7° 28'
27.5°	+ 4° 54'
25.0°	+ 2° 26'
22.5°	- 0° 6'
20.0°	- 2° 33.5'
17.5°	- 5° 6'
15.0°	- 7° 34'
12.5°	- 10° 7'
10.0°	- 12° 50.5'
7.5°	- 15° 6'
5.0°	- 17° 33'
2.5°	- 20° 8.5'

Table 7. Minimum deviation data for Mg_2Sn I

Prism drive	Sextant reading	$\frac{\alpha+\delta}{2}$ [a]	$\sin\frac{\alpha+\delta}{2}$	n [b]	λ [c]
15.20	2.5(-9.1d) [d]	20° 23'	0.34830	4.105	5.2
Slit = 0.1 millimeters			δ = 9° 54'		
Zero = 30.0°(+ 3.1d)			$\sin\frac{\delta}{2}$ = 0.08484		

[a] δ = apex angle; α = deviation angle.

[b] n = index of refraction.

[c] λ = wavelength in microns.

[d] d = 16'.

Table 8. Minimum deviation data for Mg_2Si III

$\delta = 9° 50'$

$\sin \frac{\delta}{2} = 0.08571$

zero = 30.0°(+3.2d[a]) = 8° 19.2'

slit = 0.1 millimeters

Prism drive	Sextant reading	$\frac{\alpha+\delta}{2}$ [b]	$\sin \frac{\alpha+\delta}{2}$	n[c]	λ[d]
13.25	5.0°(-1.4d)	18° 2.3'	0.30965	3.613	7.72
13.50	5.0°(-1.4d)	18° 2.3'	0.30965	3.613	7.45
13.75	5.0°(-1.7d)	18° 4.7'	0.31032	3.621	7.16
14.00	5.0°(-1.7d)	18° 4.7'	0.31032	3.621	6.86
14.25	5.0°(-2.0d)	18° 7.1'	0.31098	3.628	6.55
14.50	5.0°(-2.0d)	18° 7.1'	0.31098	3.628	6.23
14.75	5.0°(-2.2d)	18° 8.7'	0.31143	3.634	5.90
15.00	5.0°(-2.5d)	18°11.1'	0.31209	3.641	5.52
15.25	5.0°(-2.5d)	18°11.1'	0.31209	3.641	5.12
15.50	5.0°(-2.8d)	18°13.5'	0.31275	3.649	4.70
15.75	5.0°(-3.0d)	18°15.1'	0.31319	3.654	4.26
16.00	5.0°(-3.5d)	18°19.1'	0.31430	3.667	3.77
16.25	5.0°(-3.9d)	18°22.3'	0.31518	3.677	3.25
16.50	5.0°(-4.5d)	18°27.1'	0.31651	3.693	2.65
16.60	5.0°(-5.0d)	18°31.1'	0.31761	3.706	2.40
16.75	5.0°(-5.2d)	18°32.7'	0.31806	3.711	2.35
17.00	5.0°(-6.0d)	18°39.1'	0.31982	3.731	2.10
17.25	5.0°(-7.2d)	18°48.7'	0.32247	3.762	1.90

[a] d = 16'.

[b] α = deviation angle; δ = apex angle.

[c] n = index of refraction.

[d] λ = wavelength in microns.

Table 9. Minimum deviation data for Mg_2Ge I

$\delta = 10^\circ\ 00'$

$\sin \frac{\delta}{2} = 0.08716$

zero = $30.0^\circ(+3.2d^a) = 8^\circ\ 19.2'$

slit = 0.1 millimeters

Prism drive	Sextant reading	$\frac{\alpha+\delta}{2}$ [b]	$\sin \frac{\alpha+\delta}{2}$	n [c]	λ [d]
15.25	5.0°(-6.2d)	18° 45.7'	0.32164	3.690	5.12
15.50	5.0°(-6.2d)	18° 45.7'	0.32164	3.690	4.70
15.75	5.0°(-6.7d)	18° 49.7'	0.32274	3.703	4.26
16.00	5.0°(-6.7d)	18° 49.7'	0.32274	3.703	3.77
16.25	5.0°(-7.0d)	18° 52.1'	0.32340	3.723	3.25
16.50	5.0°(-7.5d)	18° 56.1'	0.32450	3.723	2.65
16.60	5.0°(-7.6d)	18° 56.9'	0.32472	3.726	2.40
16.75	5.0°(-8.1d)	19° 0.9'	0.32582	3.738	2.35
17.00	5.0°(-9.0d)	19° 8.1'	0.32780	3.761	2.10

[a] d = 16'.

[b] α = deviation angle; δ = apex angle.

[c] n = index of refraction.

[d] λ = wavelength in microns.

XI. APPENDIX D: REFLECTIVITY DETERMINATION DATA

Table 10. Reflectivity data - CsI prism (PD = prism drive; Z = corrected zero; V = maximum voltage reading; D = voltage difference; R = reflectivity)

	Al			Mg_2Sn				Mg_2Si			
PD	Z	V	D	Z	V	D	R	Z	V	D	R
13.10	12.2	28.2	16.0	5.1	22.3	17.2	1.08	3.5	11.0	7.5	0.47
13.20	12.0	30.0	18.0	5.1	23.9	18.8	1.04	3.8	11.4	7.6	0.42
13.30	13.3	32.6	19.3	4.6	26.5	21.9	1.14	4.0	12.2	8.2	0.43
13.40	13.7	35.7	22.0	5.4	30.2	24.8	1.13	3.8	14.6	10.8	0.49
13.50	14.1	39.0	24.9	5.6	32.7	27.1	1.09	4.0	15.5	11.5	0.46
13.60	13.9	43.1	29.2	6.3	35.3	29.0	0.99	3.8	17.5	13.7	0.47
13.70	16.5	45.3	28.8	7.1	37.0	29.9	1.04	4.8	18.4	13.6	0.47
13.80	18.6	48.8	30.2	7.8	38.9	31.1	1.03	4.7	19.0	14.3	0.47
13.90	16.1	50.0	33.9	6.8	40.3	33.5	0.99	4.2	19.7	15.5	0.46
14.00	15.7	54.1	38.4	6.6	45.5	38.9	1.01	4.2	22.4	18.2	0.47
14.10	17.3	67.3	50.0	6.2	54.4	48.2	0.96	5.7	27.9	22.2	0.44
14.20	17.6	77.5	59.9	6.8	62.5	55.7	0.93	4.8	32.0	27.2	0.45
14.30	12.0	57.2	45.2	4.0	46.0	42.0	0.93	4.0	24.4	20.4	0.45
14.40	12.2	68.8	54.6	4.3	54.0	49.7	0.91	3.6	27.3	23.7	0.43
14.50	12.2	79.7	67.5	4.2	63.2	59.0	0.87	3.2	33.8	30.6	0.45
14.60	8.4	59.1	50.7	3.8	45.5	41.7	0.82	2.1	25.3	23.2	0.46
14.70	8.6	67.2	58.6	3.9	50.7	46.8	0.80	2.5	29.0	26.5	0.45
14.80	9.5	72.5	63.0	3.8	54.7	50.9	0.81	2.6	31.5	28.9	0.46
14.90	9.7	74.0	64.3	4.1	54.3	50.2	0.78	3.0	32.3	29.3	0.46
15.00	11.2	73.0	61.8	4.6	50.5	45.9	0.74	3.1	31.7	28.6	0.46
15.10	12.1	74.3	62.2	5.0	45.6	40.6	0.65	3.9	32.1	28.2	0.45
15.20	11.6	80.0	68.4	5.4	42.0	36.6	0.54	4.6	35.6	31.0	0.45
15.30	8.0	63.0	55.0	3.6	25.6	22.0	0.40	3.6	27.4	23.8	0.43
15.40	9.2	81.4	72.2	4.7	26.3	21.5	0.30	3.8	35.8	32.0	0.44
15.50	6.0	64.6	58.6	2.9	17.6	14.7	0.25	2.8	28.4	25.6	0.44
15.60	6.3	75.0	68.7	3.1	17.5	14.4	0.21	3.1	33.7	30.6	0.45
15.70	7.4	83.2	75.8	3.6	17.2	13.6	0.18	3.1	37.2	34.1	0.45

Table 10. (Continued)

PD	Mg_2Ge II				Mg_2Ge (2.5 Ag)			
	Z	V	D	R	Z	V	D	R
13.10	3.5	12.4	8.9	0.56	3.5	11.0	7.5	0.47
13.20	3.8	14.3	10.5	0.58	3.8	12.3	8.5	0.47
13.30	4.0	15.6	11.6	0.60	4.0	13.8	9.8	0.51
13.40	3.8	18.5	14.7	0.69	3.8	15.0	11.2	0.51
13.50	4.0	20.0	16.0	0.64	4.0	17.0	13.0	0.52
13.60	3.8	21.5	17.7	0.61	3.8	18.2	14.4	0.50
13.70	4.8	23.7	18.9	0.66	4.8	19.6	14.8	0.51
13.80	4.7	24.5	19.8	0.66	4.7	20.3	15.6	0.52
13.90	4.2	26.8	22.6	0.68	4.2	22.4	18.2	0.54
14.00	4.2	31.1	26.9	0.70	4.2	26.6	22.4	0.58
14.10	5.7	40.8	35.1	0.70	5.7	40.2	34.5	0.69
14.20	4.8	50.5	45.7	0.76	4.8	47.6	42.8	0.72
14.30	3.9	39.5	35.6	0.79	3.5	37.9	29.1	0.76
14.40	3.4	48.5	45.1	0.83	3.6	46.0	42.4	0.78
14.50	3.2	60.7	57.5	0.85	3.2	58.0	54.8	0.81
14.60	2.1	46.3	44.2	0.87	2.1	45.2	43.1	0.85
14.70	2.5	55.2	52.7	0.90	2.5	52.6	50.1	0.86
14.80	2.6	61.0	58.4	0.93	2.6	57.9	55.3	0.88
14.90	3.0	62.8	59.8	0.93	3.0	59.4	56.4	0.88
15.00	3.1	62.4	59.3	0.96	3.1	57.8	54.7	0.89
15.10	3.9	61.7	57.8	0.93	3.9	58.0	54.1	0.87
15.20	4.6	64.7	60.1	0.88	4.6	61.5	56.9	0.83
15.30	3.6	50.6	47.0	0.85	3.6	46.0	42.4	0.77
15.40	3.8	64.5	60.7	0.84	3.8	58.1	54.3	0.75
15.50	-	-	-	-	2.8	46.0	43.2	0.74
15.60	3.1	60.4	57.3	0.83	3.1	54.1	51.0	0.74
15.70	3.1	66.3	63.2	0.83	3.1	58.7	55.6	0.73
15.80	3.1	67.4	64.3	0.84	3.1	58.7	55.6	0.72
15.90	3.1	65.5	62.4	0.85	3.1	55.8	52.7	0.72
16.00	3.2	61.3	58.1	0.82	3.2	52.3	49.1	0.69

Table 10. (Continued)

PD	Al			Mg_2Sn				Mg_2Si			
	Z	V	D	Z	V	D	R	Z	V	D	R
16.10	10.0	85.5	75.5	4.6	17.8	13.2	0.18	3.4	42.8	39.4	0.52
16.20	-	-	-	-	-	-	-	-	-	-	-
16.30	6.8	75.5	68.7	3.2	14.6	11.4	0.17	2.4	41.2	38.8	0.57
16.40	6.8	87.2	80.4	3.1	17.5	14.4	0.18	2.4	52.7	50.3	0.58
16.50	4.7	66.5	61.8	2.5	13.5	11.0	0.18	1.9	38.7	36.8	0.60
16.60	4.7	70.3	64.6	2.1	15.1	13.0	0.20	1.6	44.1	42.5	0.67
16.70	0.0	45.0	45.0					-	-	-	-
16.80	0.0	48.4	48.4					0.0	37.5	37.5	0.78
16.90	0.0	24.5	24.5					0.0	20.3	20.3	0.83
17.00	0.0	32.8	32.8					0.0	30.0	30.0	0.92
17.10	0.0	52.5	52.5					0.0	46.9	46.9	0.89
17.20	0.0	70.0	70.0					0.0	56.0	56.0	0.80
17.30	0.0	79.0	79.0					0.0	59.3	59.3	0.75
17.40	0.0	62.0	62.0					0.0	43.4	43.4	0.70
17.50	0.0	69.0	69.0					0.0	40.7	40.7	0.59
17.60	0.0	75.0	75.0					0.0	43.2	43.2	0.58
17.70	0.0	72.0	72.0					-	-	-	-
17.80	0.0	79.5	79.5					0.0	46.0	46.0	0.58
17.90	0.0	65.0	65.0					0.0	33.8	33.8	0.52
18.00	0.0	72.8	72.8					0.0	22.0	22.0	0.30
18.10	0.0	71.0	71.0					0.0	6.0	6.0	0.09
18.20	0.0	66.5	66.5					0.0	4.4	4.4	0.07
18.30	0.0	72.3	72.3					0.0	7.2	7.2	0.10
18.40	0.0	89.0	89.0					0.0	11.7	11.7	0.13
18.50	0.0	64.3	64.3					0.0	10.0	10.0	0.16
18.60	0.0	76.5	76.5					0.0	13.2	13.2	0.17
18.70	0.0	87.5	87.5					0.0	16.3	16.3	0.19
18.80	0.0	63.0	63.0					0.0	12.3	12.3	0.20
18.90	0.0	71.0	71.0					0.0	14.6	14.6	0.21
19.00	0.0	94.5	94.5					0.0	21.0	21.0	0.22

Table 10. (Continued)

PD	Mg_2Ge II				Mg_2Ge (2.5 Ag)			
	Z	V	D	R	Z	V	D	R
16.10	3.4	60.0	56.6	0.75	3.4	51.3	47.9	0.63
16.20	-	-	-	-	-	-	-	-
16.30	2.4	36.6	34.2	0.50	2.4	34.9	32.5	0.47
16.40	2.4	33.6	31.2	0.39	2.4	36.8	34.4	0.43
16.50	1.9	18.4	16.5	0.27	1.9	23.7	21.8	0.35
16.60	1.6	15.0	13.4	0.21	1.6	23.0	21.4	0.33
16.70	1.7	10.5	8.8	0.13	1.7	20.8	19.1	0.28
16.80	0.0	3.7	3.7	0.08	0.0	10.0	10.0	0.21
16.90	0.0	2.4	2.4	0.10	0.0	5.1	5.1	0.21
17.00	0.0	3.8	3.8	0.12	0.0	7.0	7.0	0.21
17.10	0.0	6.6	6.6	0.13	0.0	9.6	9.6	0.18
17.20	0.0	9.3	9.3	0.13	0.0	12.2	12.2	0.17
17.30	0.0	12.3	12.3	0.16	0.0	12.5	12.5	0.16
17.40	0.0	10.0	10.0	0.16	0.0	12.0	12.0	0.19
17.50	-	-	-	-	0.0	12.7	12.7	0.18
17.60	0.0	13.8	13.8	0.18	0.0	14.2	14.2	0.19
17.70	0.0	14.0	14.0	0.19	0.0	14.1	14.1	0.20
17.80	0.0	16.0	16.0	0.20	0.0	17.0	17.0	0.21
17.90	0.0	12.8	12.8	0.20	0.0	13.3	13.3	0.21
18.00	0.0	15.1	15.1	0.21	0.0	15.5	15.5	0.21
18.10	0.0	15.6	15.6	0.22	0.0	16.5	16.5	0.23
18.20	0.0	14.7	14.7	0.22	-	-	-	-
18.30	0.0	16.1	16.1	0.22	0.0	16.2	16.2	0.23
18.40	0.0	20.2	20.2	0.23	0.0	20.8	20.8	0.23
18.50	0.0	14.7	14.7	0.23	0.0	15.5	15.5	0.24
18.60	0.0	17.6	17.6	0.23	0.0	18.4	18.4	0.24
18.70	0.0	20.9	20.9	0.24	0.0	22.0	22.0	0.25
18.80	-	-	-	-	0.0	16.2	16.2	0.26
18.90	0.0	17.5	17.5	0.25	0.0	18.5	18.5	0.26
19.00	0.0	24.2	24.2	0.26	0.0	26.0	26.0	0.28

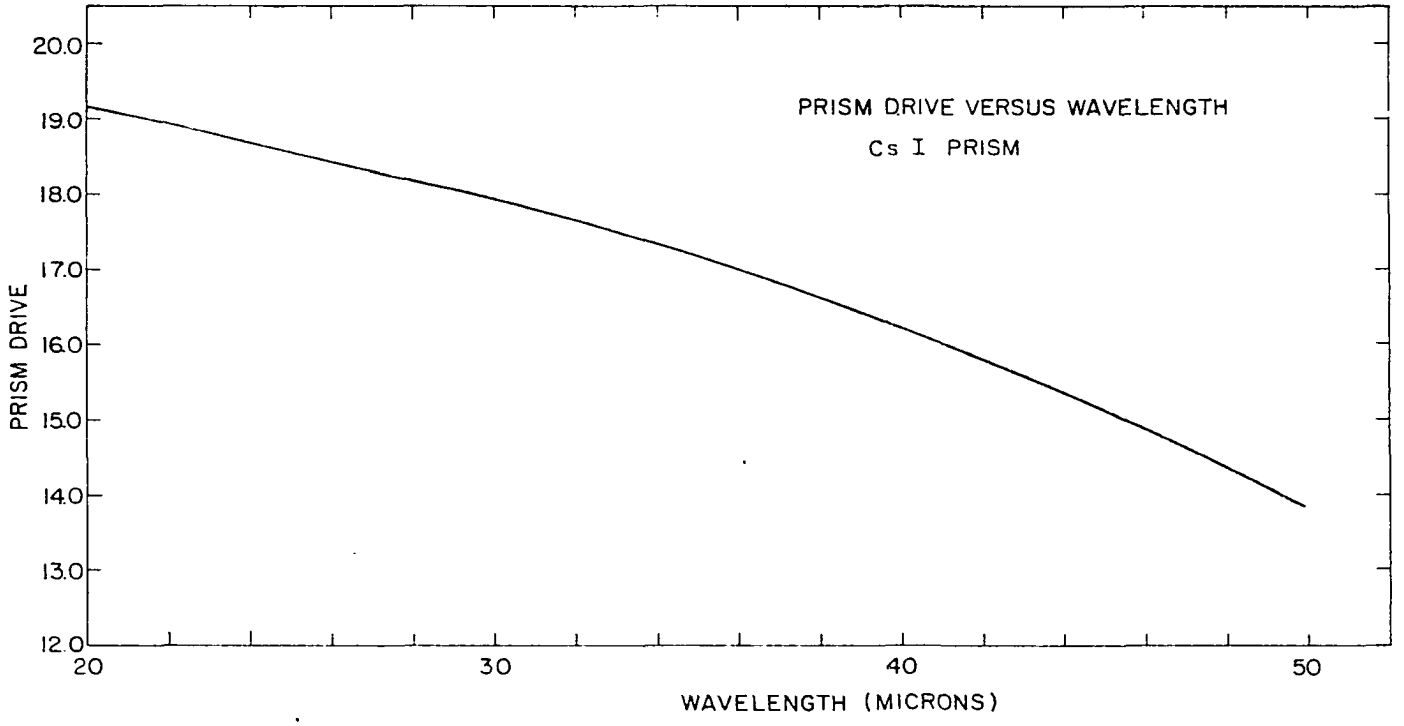

Figure 24. Approximate wavelength calibration for a 12° CsI prism in the Perkin-Elmer Model 160 monochromator. Hg green line at prism drive 23.0